COO-1198-583

SPIN-FLIP SCATTERING OF CONDUCTION ELECTRONS FROM IMPURITIES IN MOLTEN SODIUM

Edward Kevin Cornell

Department of Physics and Materials Research Laboratory

University of Illinois, Urbana, Illinois

February 1969

This is a technical information document based on a thesis submitted by Edward Kevin Cornell in partial fulfillment of the requirements for the degree of Doctor of Philosophy in Physics in the Graduate College of the University of Illinois 1969. The research was supported in part by the U. S. Atomic Energy Commission under Contract AT(11-1)-1198.

SPIN-FLIP SCATTERING OF CONDUCTION ELECTRONS FROM IMPURITIES IN MOLTEN SODIUM

Edward Kevin Cornell, Ph.D.
Department of Physics
University of Illinois, 1969

The effects of four new impurities (Bi, Pt, Pd, and Ag) on the conduction electron spin resonance signal of sodium metal has been observed. Due to solubility problems, previous attempts to see effects from these impurities have been unsuccessful. By going into the molten state these problems were surmounted. The spin-flip scattering cross section of these impurities was determined. The cross section for bismuth is of particular interest in that it serves as a test of the "resonance hypothesis" theory proposed by Ferrel and Prange. In addition to scattering cross sections, the equilibrium solubilities of bismuth and palladium were determined as a function of temperature. These curves were used to determine the entropy and enthalpy of solution for bismuth and palladium in sodium.

ACKNOWLEDGMENTS

It is a pleasure to acknowledge the author's indebtness to his research advisor, Professor C. P. Slichter. Professor Slichter's enthusiasm for physics has made the author's education especially rewarding.

The author would also like to thank the staff of the Materials Research Laboratory for its professional help. Special thanks are due to Mr. Clyde Burkhead for his help in purchasing needed material and to the staff of the stockroom whose efficiency were invaluable in experimental research.

The author also acknowledges past and present members of the Slichter magnetic resonance group for their help and moral support.

Finally, the author wishes to extend his appreciation to his wife, Nina, for her patience, love and understanding during the years of graduate study.

This research was supported in part by the United States Atomic Energy Commission under Contract AEC(1480)-1198.

TABLE OF CONTENTS

LIST OF FIGURES

Figures Page

Figures Page

I. INTRODUCTION

The effect of impurities upon the properties of metals has been subject to much experimental and theoretical work during recent years.[1] One of the basic problems is to determine and account for the electronic configuration that the impurity atom assumes in the host metal. Phenomena which can be employed to study impurity atoms include resistivity,[2] Knight shift,[3] quadrupole coupling of neighboring nuclei,[4] and conduction electron spin resonance.[5,6] The latter technique was used to study dilute concentrations of substitutional impurities which dissolve in lithium and sodium only in the liquid state.

Any theoretical treatment of this problem entails Many Body considerations of the sea of conduction electrons. The study of the redistribution of conduction electrons around impurities in metals is based on the theoretical work of Friedel,[7] who analyzed the distribution of the electron gas in terms of phase shifts introduced into the partial waves of the electron wave functions by the impurities. These phase shifts measure the extent to which different angular momentum components in a partial wave decomposition of the wave functions are distorted. Compact equations express various phenomena which result from this disturbance in terms of phase shifts.

This thesis describes experiments that extend results reported by Asik, Ball and Slighter.[8] ABS determined the spin-flip scattering cross section of a number of nonmagnetic impurities in sodium and lithium. Their theoretical calculations attempting to explain an unexpected maximum in these cross sections were not successful. The present

experiments were carried out in an attempt to extend ABS's data on non-magnetic impurities in hopes of shedding new light on the mechanism causing this peak.

Information on four new impurities (bismuth, silver, gold and palladium) in sodium was obtained. ABS were unable to see any effect of these impurities on the conduction electron spin resonance of sodium. This was a result of their measurements being made at room temperature where sodium is in the solid state and where these impurities will not stay dissolved. This problem was surmounted by carrying out the present experiments at higher temperatures where sodium is liquid.

The data obtained did not lead to any new calculations which could explain the position of the maximum, although further theoretical considerations are presented in the last section of this chapter. However, this data did serve as a crucial test of a semi-quantitative curve-fitting solution suggested by Ferrel and Prange.[9] By fitting ABS's data for gold row impurities, FP predicted the spin-flip scattering cross section for bismuth, but unfortunately ABS had not succeeded in dissolving bismuth in sodium. By going to the molten state the present experiments succeeded in determining this cross section which serves as a test of the FP theory.

In addition to the spin-flip scattering cross section, the equilibrium soluble concentrations of palladium and bismuth as a function of temperature were determined for temperatures up to 250°C.

Very little background material is presented in this thesis for if given here it would only duplicate that contained in Asik's thesis.[10] The second section contains a brief review of ABS's results and some

calculations that were made in an attempt to check their theoretical calculations with other experimental data on resistivity and Knight shift measurements contained in the literature. The experimental apparatus and technique are presented in section three. The experimental results are given in section four. Section five is concerned with theoretical considerations.

II. CESR, RESISTIVITY, AND KNIGHT SHIFT IN ALLOYS

A. CESR

The first paramagnetic resonance absorption in metals due to conduction electrons was observed in 1952 by Griswold, Kip and Kittel.[11] Since then, it has been observed in Li, K, Be,[12] Cs,[13] Rb,[14,15] Cu,[16] Al,[17] and Ag.[18]

A systematic study of the effect of impurities on the CESR signal in Li and Na has been done by Asik, Ball and Slichter.[8] They measured the dependence of the CESR linewidth on type and concentration of impurities in solid solution. For fourteen impurities in Li and seven impurities in Na they were able to see a broadening effect on the CESR linewidth. The large spin-orbit coupling of high Z elements such as Au and Tl produced measurable effects for concentrations as low as one atom in 10.[7]

For some impurities solubility limits were found. The linewidth increased with concentration up to a certain concentration beyond which no further broadening was observed. For other impurities no broadening was observed. Here it was assumed that not even extremely dilute concentrations were soluable. In still other cases it was found that the sample deteriorated as a function of time. There was a sharp decrease in linewidth over a period of several weeks for a few alloy systems (LiSn, LiPb). An alloy sample having an initial linewidth of 150 gauss was found to have a linewidth of one to five gauss upon measurement a few weeks later. It was precisely this behavior that led to our considerations of making high temperature measurements. For if some samples will

precipitate out of solution in a few weeks, others might do so in a few seconds, hence no broadening would be seen in the solid state.

ABS were able to account for the experimental results for monovalent impurities, such as Au and Ag, by an OPW theory which considers the interaction of the conduction electron spin with its orbital motion in the electric field of the impurity atom (spin-orbit coupling) as a perturbation. For non-monovalent impurities, they represented the electrostatic effect of the impurity by a screened coulomb potential and again took the spin-orbit interaction as a perturbation. This theory accounts for the experimental results for impurities having valence differences of $\pm$ 1 with respect to Li and Na. However, for the high atomic Z elements of Groups IIIA and IVA this simple theory deviates from the results. When the valence difference becomes +3 the experimental results decrease while the theoretical ones increase. This maximum is exhibited in the Au and Ag rows in both Na and Li.

In an attempt to describe this resonance behavior ABS developed an alternate theory. The problem was set up in the Jl representation where the spin flip scattering cross section can be written as

$$\sigma_{sF} = \frac{8\pi}{k_F^2 3} \sum_{\ell} \frac{\ell(\ell+1)}{2\ell+1} \sin^2 \left(\delta^{\ell}_{J-1/2} - \delta^{\ell}_{J+1/2} \right) \qquad (1)$$

where δ^{ℓ}_{J} is the partial wave phase shift for orbital angular momentum ℓ and total angular momentum J.[19] To calculate these phase shifts a model for the potential surrounding the impurity atom in the host metal was assumed. This potential consisted of the free impurity atom potential

out to a radius R. Beyond R the potential was taken as flat and coinciding with the bottom of the conduction band. The Schrodinger equation was then numerically integrated at an energy equal to the known Fermi energy above the bottom of the band, and the s, ρ, and d phase shifts were determined. The Freidel sum was then computed and the radius R was adjusted so that the phase shifts satisfied the Friedel sum rule. This theory does predict a maximum in the spin flip scattering cross section but it occurs at the s^2p^3 atomic configuration which corresponds to a +4 relative valence. The experimental cross sections peak between +3 and +2 relative valence.

B. Resistivity

Electrical resistivity measurements can be used as a means of examining electronic configurations of impurity atoms in metals. The impurity induced resistivity can be written in terms of the partial wave phase shifts. The formula for resistivity[20] is

$$\frac{4\pi}{e^2 k_F} \sum \ell \sin^2(\delta_{\ell-1} - \delta_\ell) \tag{2}$$

when spin-orbit coupling is neglected, and

$$\frac{4\pi}{e^2 k_F} \sum_{\ell=1}^{\infty} \frac{(\ell+1)}{(2\ell+1)(2\ell+3)} \left\{ \sum_{jj'} (j+1/2)(j'+1/2) \sin^2\left(\delta_j^{\ell+1/2} - \delta_{j'}^{\ell}\right) \right.$$

$$\left. + 2\ell \sin^2\xi_\ell - 2\ell(\ell+1)\sin\xi_\ell \sin\xi_{\ell+1} \cos\left(\delta^{\ell}_{\ell+1/2} + \delta^{\ell}_{\ell-1/2} - \delta^{\ell+1}_{\ell+1/2} + \delta^{\ell+1}_{\ell+3/2}\right) \right\} \tag{3}$$

where $$\xi_\ell \equiv \left(\delta^{\ell}_{\ell+1/2} - \delta^{\ell}_{\ell-1/2}\right) \tag{4}$$

when it is not.

Taking existing data on impurity-induced resistivity in Na and L_i, a comparison can be made with the values predicted by ABS. The results of these calculations are shown in Table I. Including the spin-orbit interaction does improve agreement in all of the calculations. The agreement between theory and experiment is rather poor for LiSn and NaAu. Notice, however, that the theory does distinguish between NaSn and NaPb with fairly good agreement. This is in contrast to spin-flip scattering calculations using the same phase shifts which do not distinguish between the two. At this point one might well wonder why there is such a large discrepancy between predicted and experimental values for spin-flip scattering cross section when resistivity calculations for the same systems are fairly good. The answer lies in the fact that the largest contribution to resistivity comes from s wave scattering. Spin-flip scattering on the other hand has no s wave contribution. This can be easily seen by noting that the spin-orbit interaction, which produces the spin flip, is proportional to ℓ and is zero for $\ell = 0$. Thus if S wave phase shifts are correct, resistivity calculations will be good. On the other hand, spin-flip cross sections may be incorrect due to an error in p and d wave phase shifts. This is illustrated by taking ABS's phase shifts and introducing a .1% change in the p wave phase shift. The result is a 2% change in spin-flip cross section and a .1% change in resistivity. Thus, CESR is a more sensitive probe of the p wave electronic configuration of an impurity than resistance.

Due to the difficulty with which large amounts of impurities will disolve in Li and Na, the existing data on impurity-induced resistance is meager. If one goes to other systems, behavior similar to that of the

Table I

Resistivity Calculations

	Calculations		Experimental	Ref.
	without spin orbit	with spin orbit	Results	
LiMg	1.06	1.04	.83	24
LiAl	4.08		4. $\pm$ 1	23
LiIn	4.31	4.42	8.6	23
LiSn	7.54	8.66	1	24
NaAu	.21	.23	5	25
NaCl	2.84	2.94	5	25
NaTl	6.06	7.5	11	26
NaSn	10.2	10.21	10.2	25
NaPb	10.00	11.8	11.6	25

spin-flip scattering cross section in Li and Na can be found. Vassel[21] found that selenium impurities in copper produced a smaller value of residual resistivity than arsenic. Coqblen et al.[22] studied the resistivity and thermoelectric power of silver base alloys containing selenium and krypton. When combined with previous data, the valence dependence of the resistivity of copper row (Cu-Kr) impurities in silver has a resonant shape with a peak at arsenic. The thermoelectric power behaves anomalously, going to zero between arsenic and selenium.

C. Knight Shift

A change in the Knight shift, the shift of resonance frequency of the nuclei of the host metal atoms, is another phenomenon which can be analyzed from the standpoint of partial wave phase shifts. In this case[27] the fractional change in Knight shift per unit concentration becomes

$$\frac{1}{k}\frac{\partial k}{\partial c} = \sum_{\ell} A_{\ell} \sin^2 \delta_{\ell} + B_{\ell} \sin 2\delta_{\ell} \qquad (5)$$

$$A_{\ell} = \int_0^{\infty} (2\ell+1)\rho(r)\, \eta_{\ell}(k_F r) - j_{\ell}^2 (k_F r)\, dr \qquad (6)$$

$$B_{\ell} = \int_0^{\infty} (2\ell+1)\rho(r)\, \eta_{\ell}(k_F r)\, j_{\ell}(k_F r)\, dr \qquad (7)$$

where n_{ℓ} and j_{ℓ} are respectively the spherical Newman and Bessel functions of order 1 and p(r), p(r) is the radial distribution function of the nuclei around the impurity atom (the probability of finding a nucleus in a volume at a distance r from an impurity atom). In solids p(r) is determined by the lattice structure. In liquids it is determined experimentally from X-ray, electron, and neutron scattering.

Hanabusa and Bloembergen[28] have made a study of the change in Knight shift resulting from impurities in Na. Here also one finds a peak in the Knight shift around Tl and a smaller value for Pb. Figure (1) shows the experimental results in comparison with theoretical calculations made from ABS's phase shifts. Here again ABS's theory is unable to explain the maximum.

Figure 1. The fractional Knight shift change for unit solute concentrations of impurities in sodium.

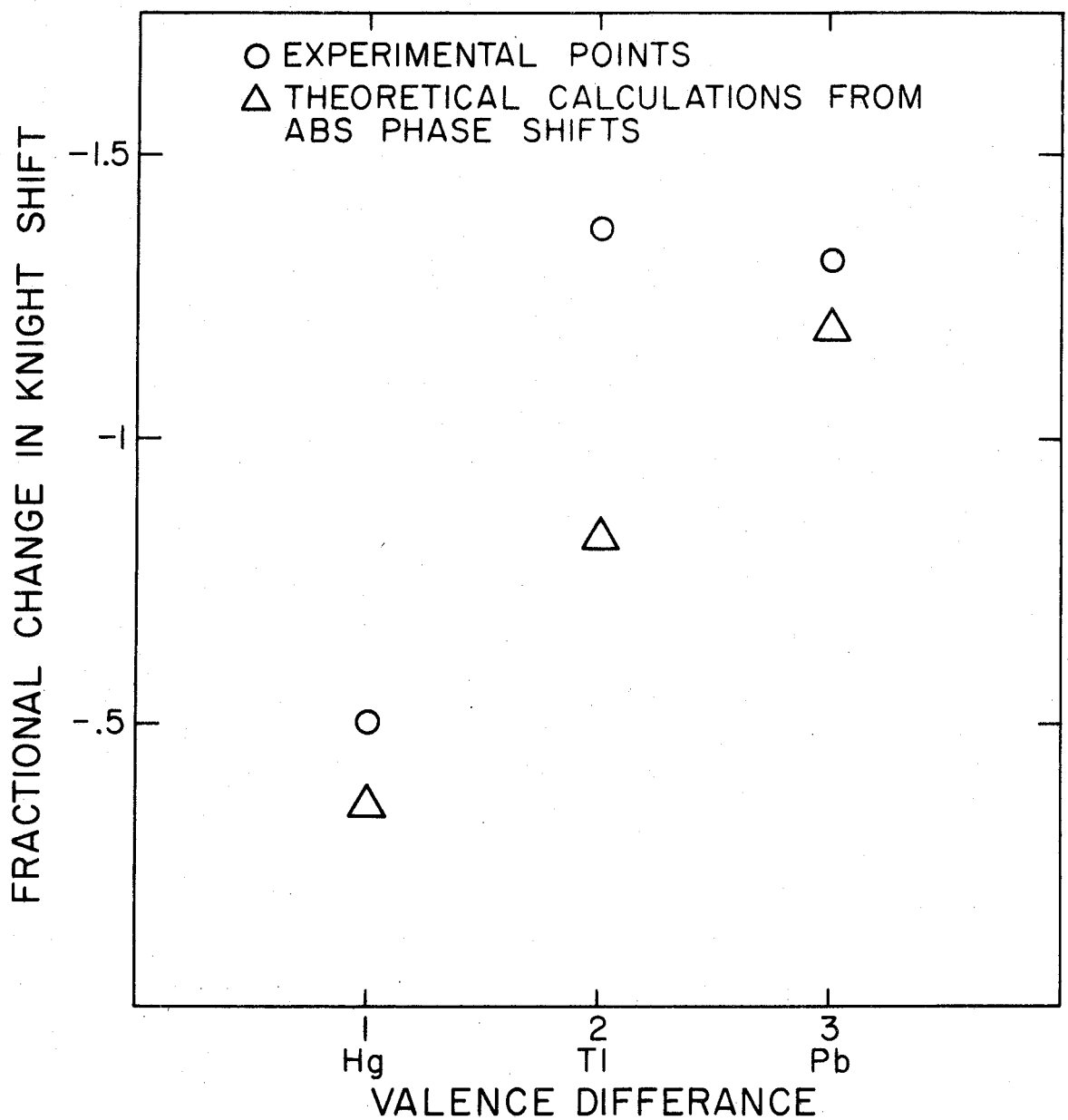
O EXPERIMENTAL POINTS
Δ THEORETICAL CALCULATIONS FROM ABS PHASE SHIFTS
FRACTIONAL CHANGE IN KNIGHT SHIFT
-1.5
-1
-.5
1
Hg
2
Tl
3
Pb
VALENCE DIFFERANCE

III. EXPERIMENTAL APPARATUS AND TECHNIQUE

A. Sample Preparation

The alkali metal alloys were prepared in the following manner. The surface of the alkali metal was cleaned, the metal weighed, and a small piece of previously weighed impurity metal was embedded in the alkali. This was all done in a Kewaunee Scientific Co. controlled atmosphere dry box, which was equipped with a recirculation system. The recirculation system continuously dried the interior of the enclosure by internal circulation of the dry atmosphere through tubes containing calcium sulphate dessicant. The internal atmosphere consisted of nearly 100% pure argon.

The host alkali with impurity embedded in it was then dropped in mineral oil in a stainless steel cup and alloyed on a hot plate for at least three hours.

Next, this alloy was dispersed in mineral oil by a high-speed stirring apparatus constructed by Joe Asik. This consisted of a 10,000 rpm 1/7 hp motor driving a stainless steel stirring rod. The rod extended down into the center of a three-necked flask through a double "o" ring seal. About 10cc of metal and 100cc of mineral oil were heated in the flask under an argon atmosphere to above the melting point of the host metal. Then the stirring was done while the flask cooled. Coagulation was prevented if a small amount of outside atmosphere was allowed to seep into the flask while it was cooling. This last step was in lieu of using about 0.35cc of oleic acid.

Most of the mineral oil was next removed by centrifuging. Then the rather thick paste was drawn up into a sample tube and sealed off.

For sodium, a 2mm I.D. and 4mm O.D. quartz tube about ten inches long was used. This was sealed at each end with a blow torch.

B. High Temperature Water-Cooled Cavity

The molten state CESR measurements were made in an X band resonant cavity which is designed to operate at temperatures as high as 1200°C. It consists of a platinum-coated quartz tube resistively heated inside a water-cooled cavity.

Other systems have been used for high temperature resonance measurements, but each has its limitations. Hot gas blowers can be used to obtain temperatures up to 300°C. With an oven surrounding the entire cavity, temperatures of about 600°C can be obtained. A more attractive scheme consists of a heater made up of vertical wires inside a rectangular cavity. This arrangement will reach temperatures of about 700°C.

The cavity used is shown in Figure 2.[29] It is a full-wavelength rectangular reflection cavity operating in the TE102 mode. A small iris with a slide screw was used to couple the cavity to the microwave transmission line. Both the flange and the cylindrical brass heater tube supports were silver-soldered to the cavity. The brass water cooling jacket was soft-soldered. A water flow rate of about 400 cm^3/min was sufficient to keep the cavity at room temperature for operating temperatures up to 1200°C.

The size of the quartz heater tube is not critical. In this experiment a 6mm O.D. tubing with 1mm wall thickness was used. The resistive heating elements consisted of two strips of platinum about 1/16 inches wide bonded to the quartz on opposite sides of the tube. To obtain these bonded strips, platinum paste[30] was applied with a fine

Figure 2. Water cooled high temperature cavity.

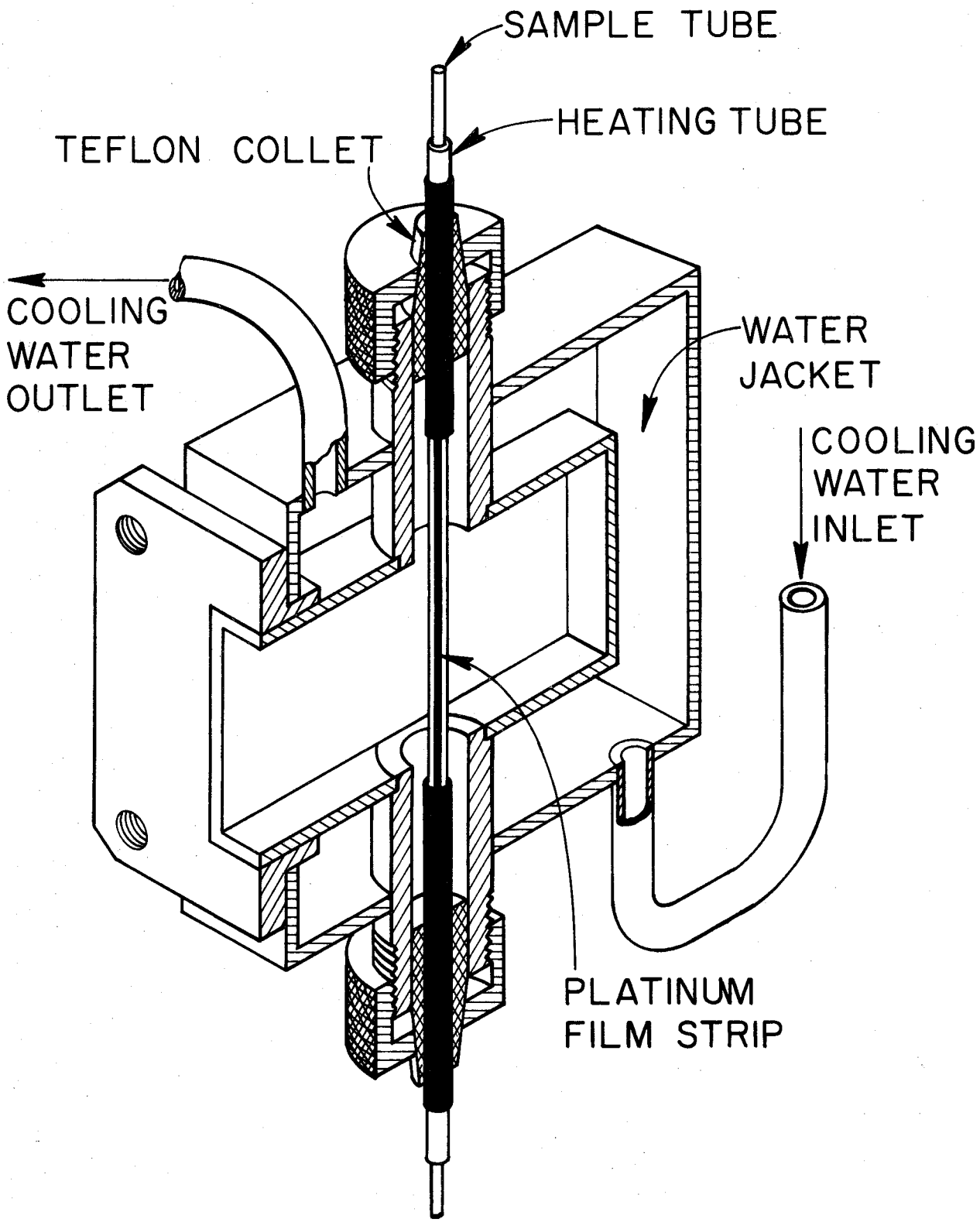
SAMPLE TUBE
HEATING TUBE
TEFLON COLLET
COOLING
WATER
OUTLET
WATER
JACKET
COOLING
WATER
INLET
PLATINUM
FILM STRIP

camel's hair brush and fired in air at 650°C. The ends of the tube were completely coated with platinum so that the teflon collet holding the tube in place would not get hot. The current leads consisted of two metal nonmagnetic testube clamps which could be easily attached and removed.

The room temperature resistance of the heater tube was about ten ohms. In order to avoid any modulation of the cavity resonant frequency in the magnetic field, a fairly-well filtered dc power source was used for the heater. The thermal characteristics of the system are excellent. The heat capacity of the heater is so small that a stable temperature of 350°C, the highest usual running temperature, could be reached in a few minutes. The temperature gradient inside a sample tube at 350°C was found to be about 7°C over the central 3/4 inches of the cavity.

The microwave properties of the system are very good. If care is taken in orienting the heater tube so the planes of the platinum strips are perpendicular to the E vector of the microwave field in the cavity, the Q is not much different from that of the empty cavity. Also, the constant cavity temperature allows temperature runs on a sample to be made without rebalancing the spectrometer.

C. EPR Spectrometer

The CESR linewidth measurements were made using a single klystron superheterodyne EPR spectrometer. Except for a few modifications which will be described below this spectrometer is described in Joe Asik's thesis.[31]

The magnetic field modulation coils were reduced in size to 7" diameter and placed on the inside of the magnet pole pieces.

This allowed modulation amplitudes of up to 18 gauss peak to peak at a frequency of 160 cps, the frequency used.

The signal output from the lock-in detector instead of being fed directly to a chart recorder was fed into a digital signal averager (Nucleas Data Enhancentron #1024). This was done to achieve greater signal to noise and to surmount the problem of baseline drift which caused trouble during high temperature runs.

A delayed recurrent field sweep was obtained by using a Textronix #162 waveform generator in conjunction with a Textronix #161 pulse generator. Both the 161 and 162 were modified to provide a ramp from 16 to 250 seconds long, spaced at intervals from one to thirteen seconds. The field sweep interval was varied by resistance dividing the output from the 162 generator. This gave sweeps of from 20 to 1,000 gauss. To enable easy sweep calibration (gauss/second) the sweep time of the ramp was adjusted to coincide exactly with that of the Enhancentron. Usually, a sweep time of 16.384 seconds with a delay interval of 6 seconds was used. The field sweep interval was varied with signal linewidth to yield an adequate baseline. The ratio of signal to noise goes as $\sqrt{N}$, where N = number of sweeps. Thus, a sufficient number of sweeps were made to yield a signal to noise ratio of at least 25.

IV. EXPERIMENTAL RESULTS

A. Linewidths as a Function of Temperature and Concentration

A broadening of the CESR linewidth was observed in dilute alloys of four impurities in sodium at temperatures above the melting point of sodium (T_m = 97.8°C). Fourteen additional impurities were found to produce no broadening in sodium at temperatures up to 350° C. This is attributed either to an insolubility of the impurity atoms, or to a formation of a second phase which precludes formation of a dilute disordered alloy. The latter is most probably the case with antimony and tellurium since when alloyed above the melting point both are vigorously attacked by molten sodium.

There are two aspects of the experimental results that are of interest. First is the broadening factor which is the rate of change of the linewidth with respect to concentration. Second, it is possible to deduce the solubility curves of the sodium impurity system. Both are found by taking samples of known concentrations and observing how the linewidth of the CESR signal, ΔH, behaves as a function of temperature.

Below the melting point of sodium, the alloy linewidth behaves exactly the same as that of pure sodium. ΔH increases linearly with temperature. Above the melting point the impurity-doped samples behave differently from pure sodium. As can be seen in Figure 3, the pure sodium linewidth jumps by 2.8 gauss at T_m and continues to increase with the same slope above T_m. This is not the case for impurity-doped samples. In samples containing small amounts of platinum and silver the linewidth (see Figures 4 to 11) jumps by more than 2.8 gauss at T_m, and then

Figure 3. The temperature dependence of the CESR linewidth for pure sodium.

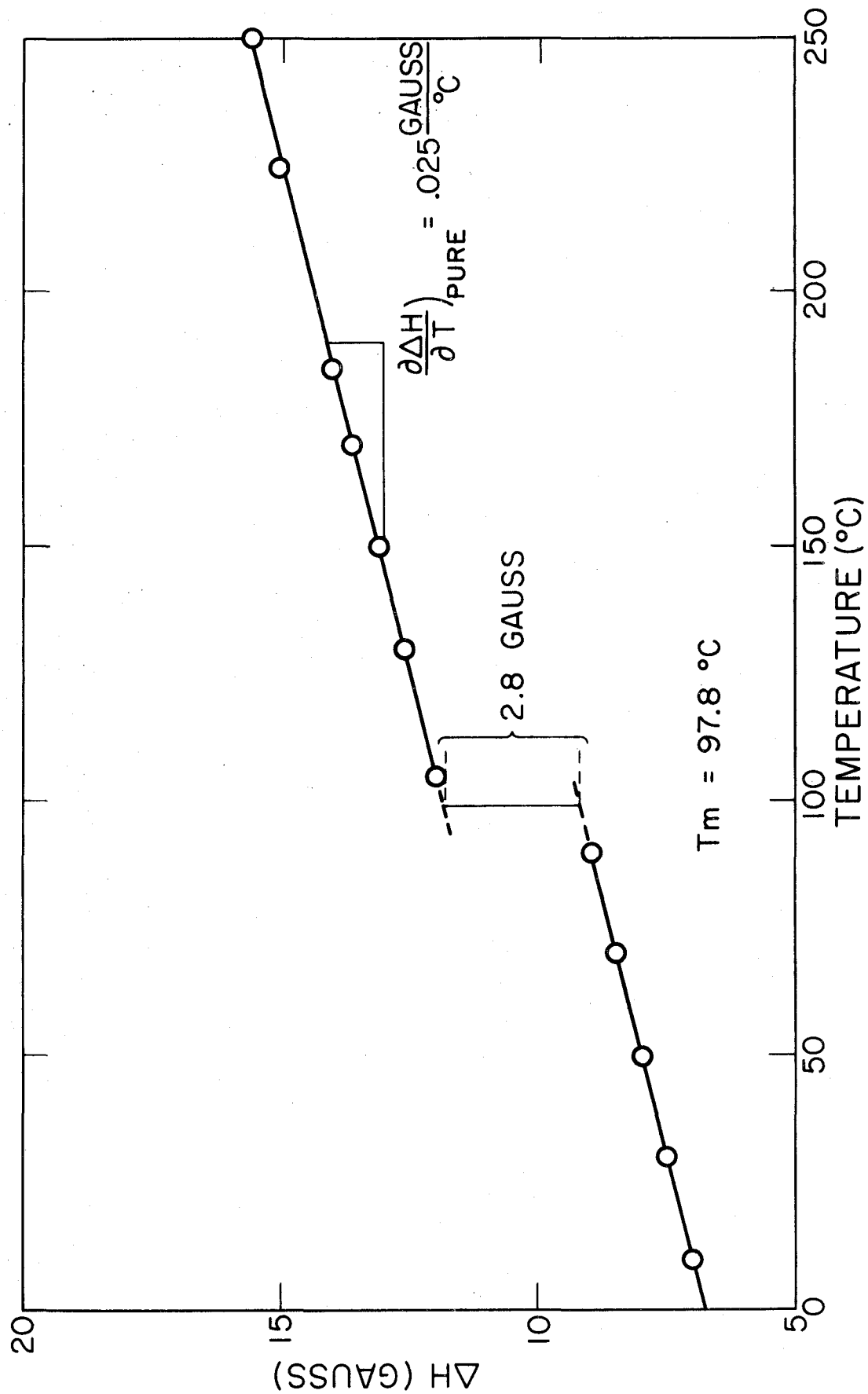
ΔH (GAUSS)
20
15
10
5
0
50
100
150
200
250
TEMPERATURE (°C)
Tm = 97.8 °C
2.8 GAUSS
$\frac{\partial \Delta H}{\partial T})_{PURE} = .025 \frac{GAUSS}{°C}$

Figure 4. The temperature dependence of the CESR linewidth of sodium doped with $(2.01 \pm .2) \times 10^{-3}$ at. % platinum.

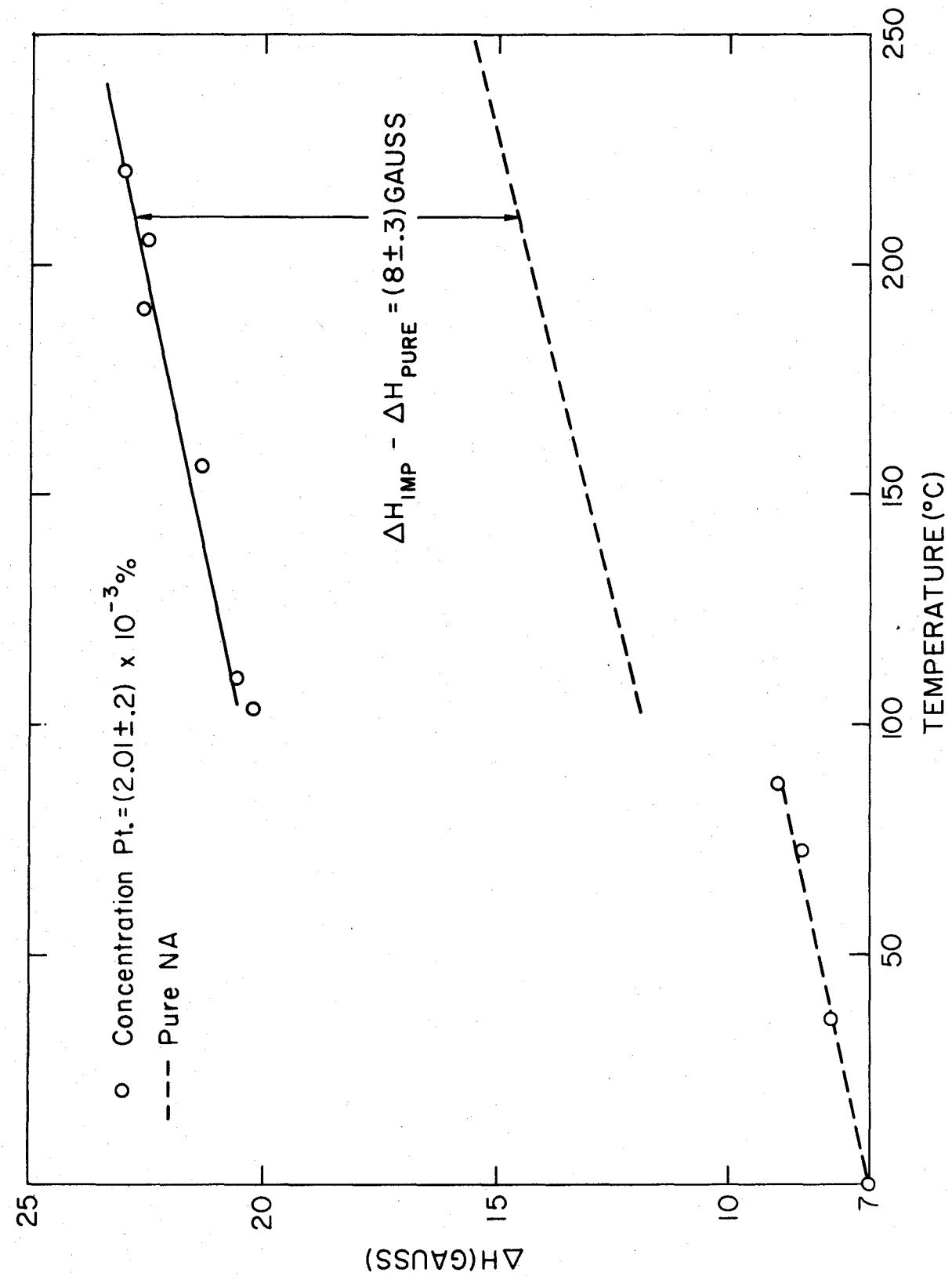
o Concentration Pt.=(2.01±.2) x 10⁻³%
--- Pure NA
ΔH_IMP - ΔH_PURE = (8±.3) GAUSS
ΔH (GAUSS)
TEMPERATURE (°C)
25
20
15
10
7
50
100
150
200
250

Figure 5. The temperature dependence of the CESR linewidth of sodium doped with $(2.71 \pm .1) \times 10^{-3}$ at. % platinum.

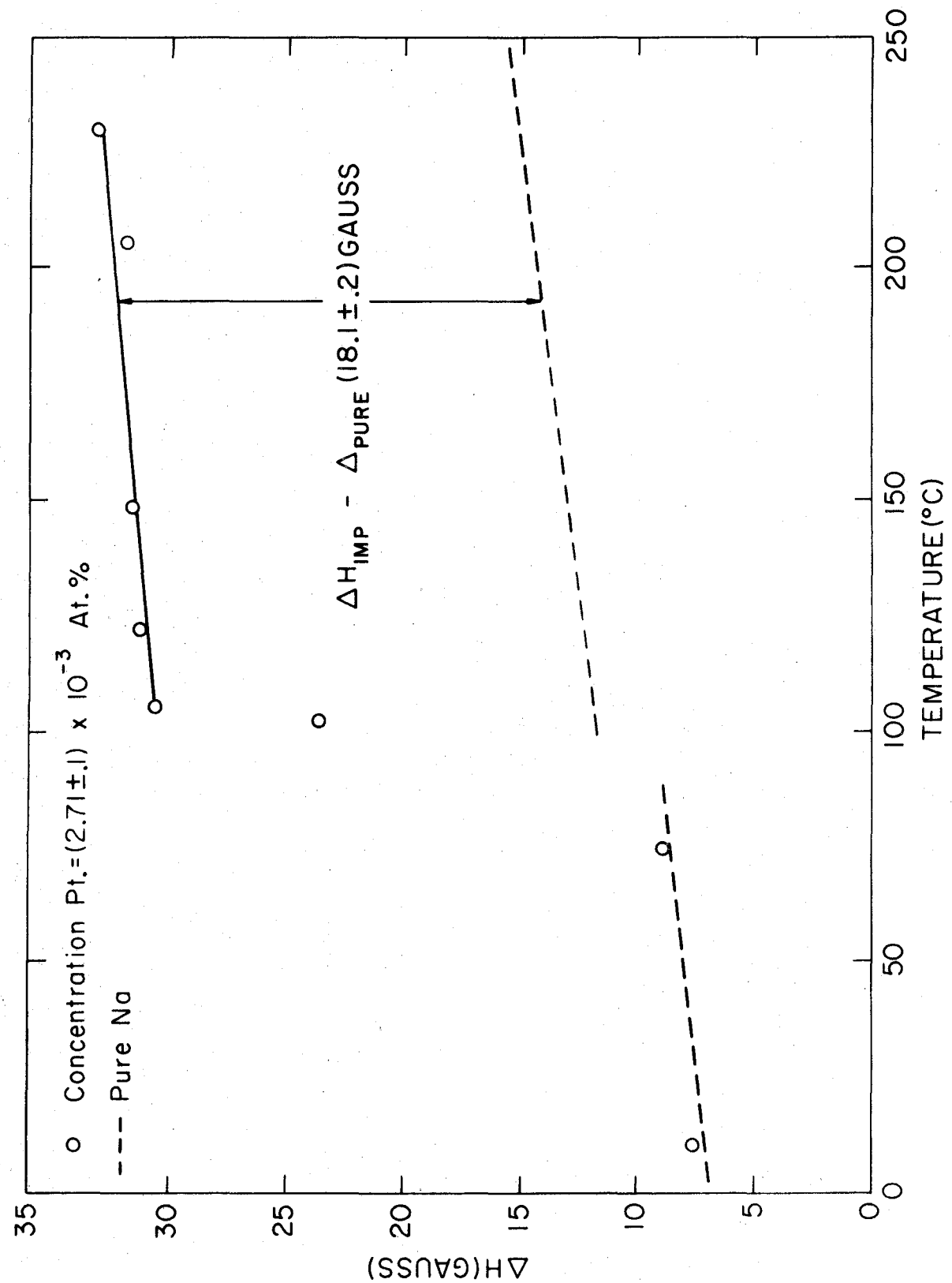
o Concentration Pt.=(2.71±.1) x 10⁻³ At.%
--- Pure Na
ΔH_IMP - Δ_PURE (18.1±.2)GAUSS
ΔH(GAUSS)
TEMPERATURE(°C)
0
5
10
15
20
25
30
35
0
50
100
150
200
250

Figure 6. The temperature dependence of the CESR linewidth of sodium doped with $(6.88 \pm .1) \times 10^{-3}$ at. % platinum.

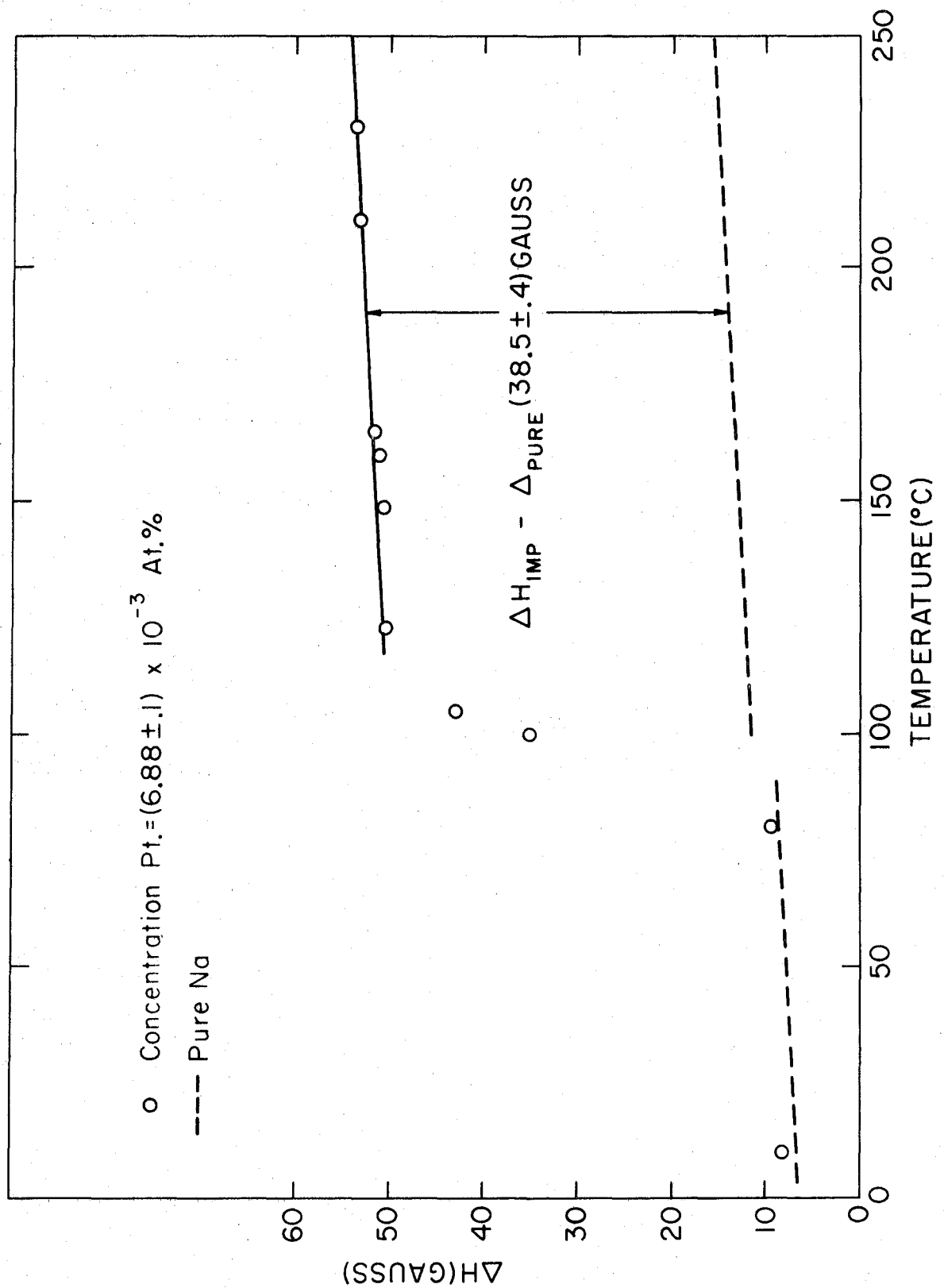
o Concentration Pt.=(6.88±.1) x 10^{-3} At.%
--- Pure Na
$\Delta H_{IMP} - \Delta_{PURE}$(38.5±.4)GAUSS
ΔH(GAUSS)
TEMPERATURE(°C)
0
10
20
30
40
50
60
0
50
100
150
200
250

Figure 7. The temperature dependence of the CESR linewidth of sodium doped with $(1.17 \pm .3) \times 10^{-3}$ at. % platinum.

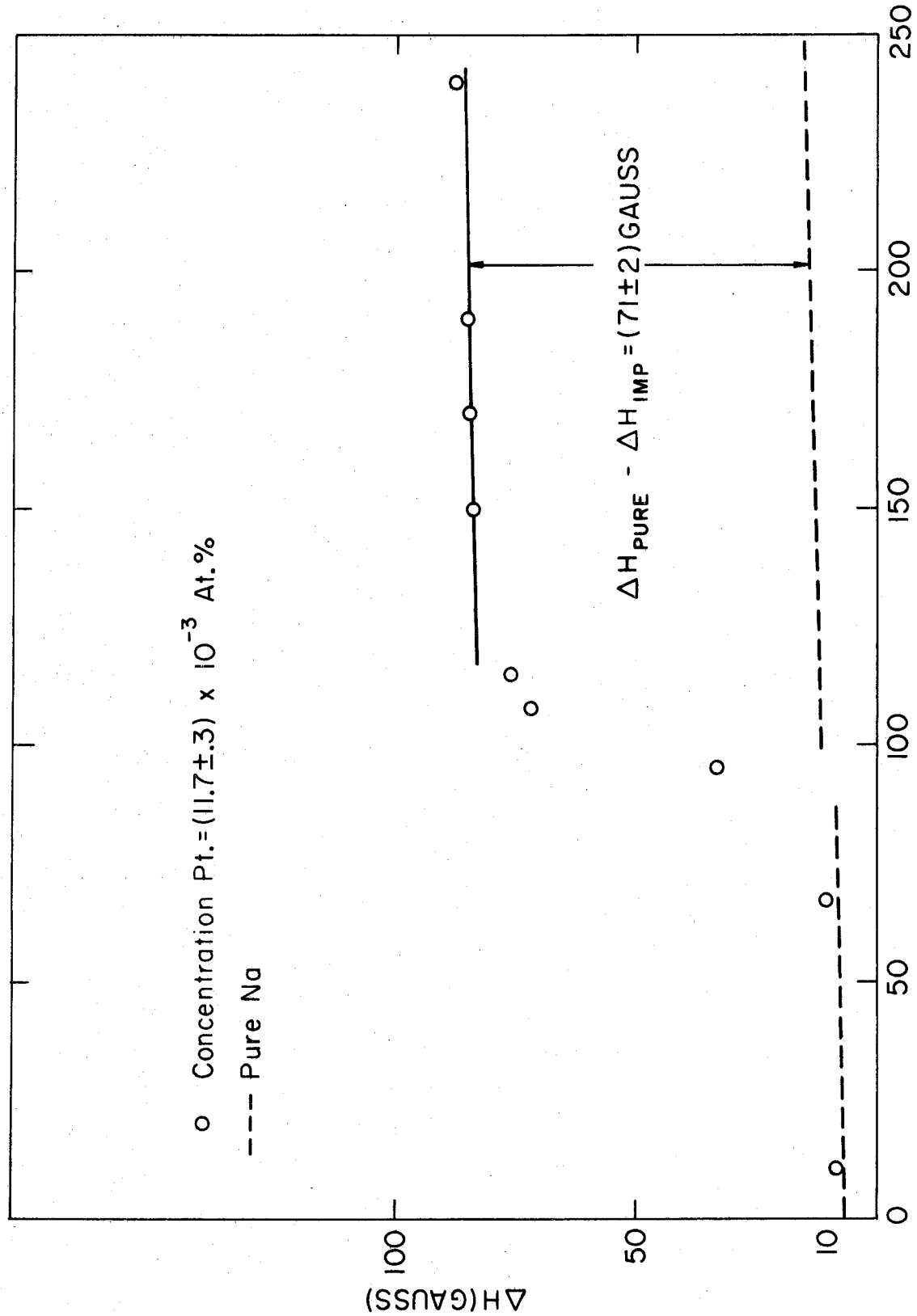
o Concentration Pt.=(11.7±.3) x 10^{-3} At.%
--- Pure Na
$\Delta H_{PURE} - \Delta H_{IMP} = (71 \pm 2)$ GAUSS
ΔH(GAUSS)
100
50
10
0
50
100
150
200
250
TEMPERATURE(°C)

Figure 8. The temperature dependence of the CESR linewidth of sodium doped with 5.5×10^{-3} at. % silver.

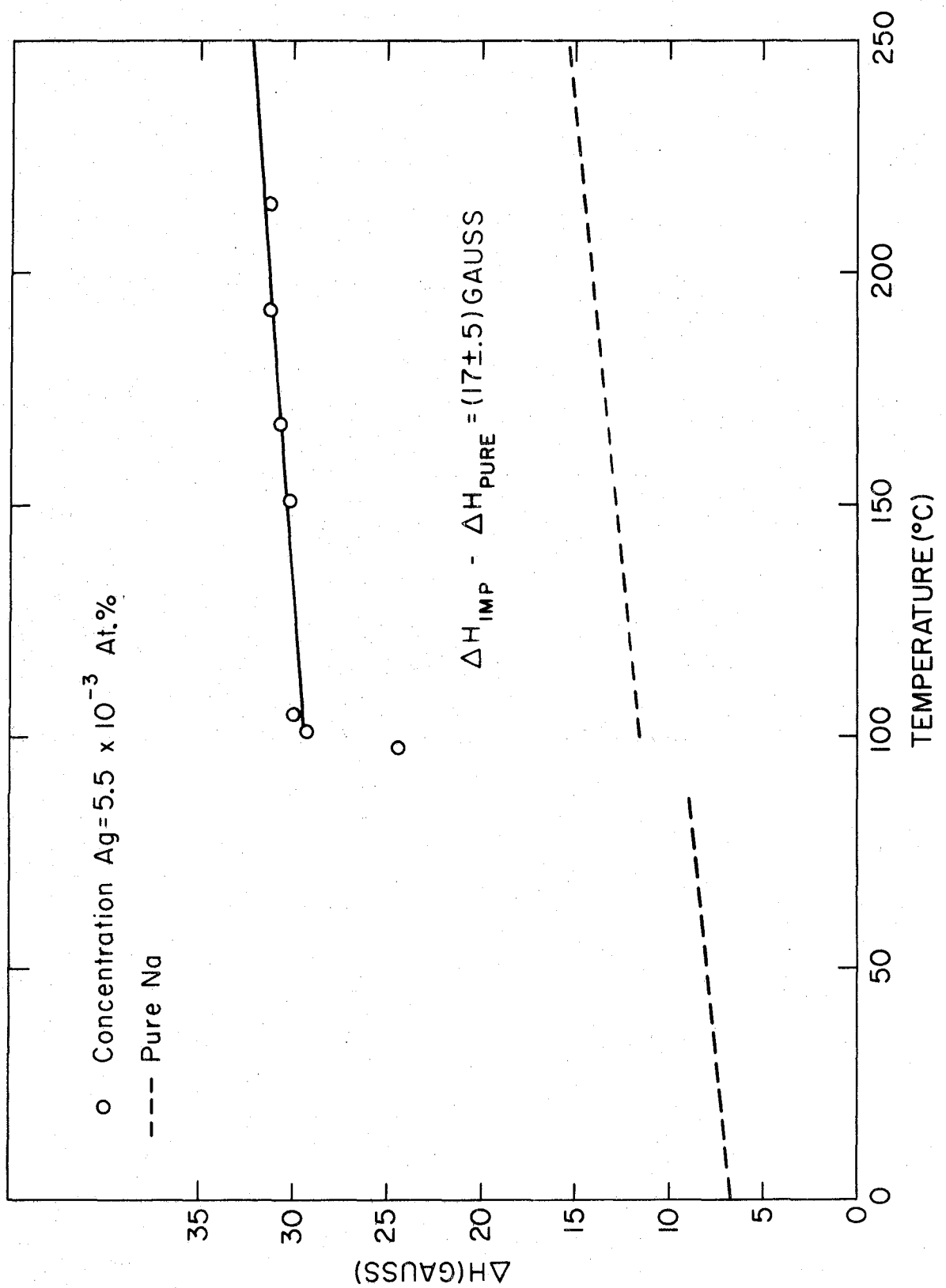
o Concentration Ag=5.5 x 10⁻³ At.%
--- Pure Na
ΔH_IMP - ΔH_PURE = (17±.5) GAUSS
ΔH(GAUSS)
TEMPERATURE (°C)
0
5
10
15
20
25
30
35
0
50
100
150
200
250

Figure 9. The temperature dependence of the CESR linewidth of sodium doped with $(10.3 \pm .3) \times 10^{-3}$ at. % silver.

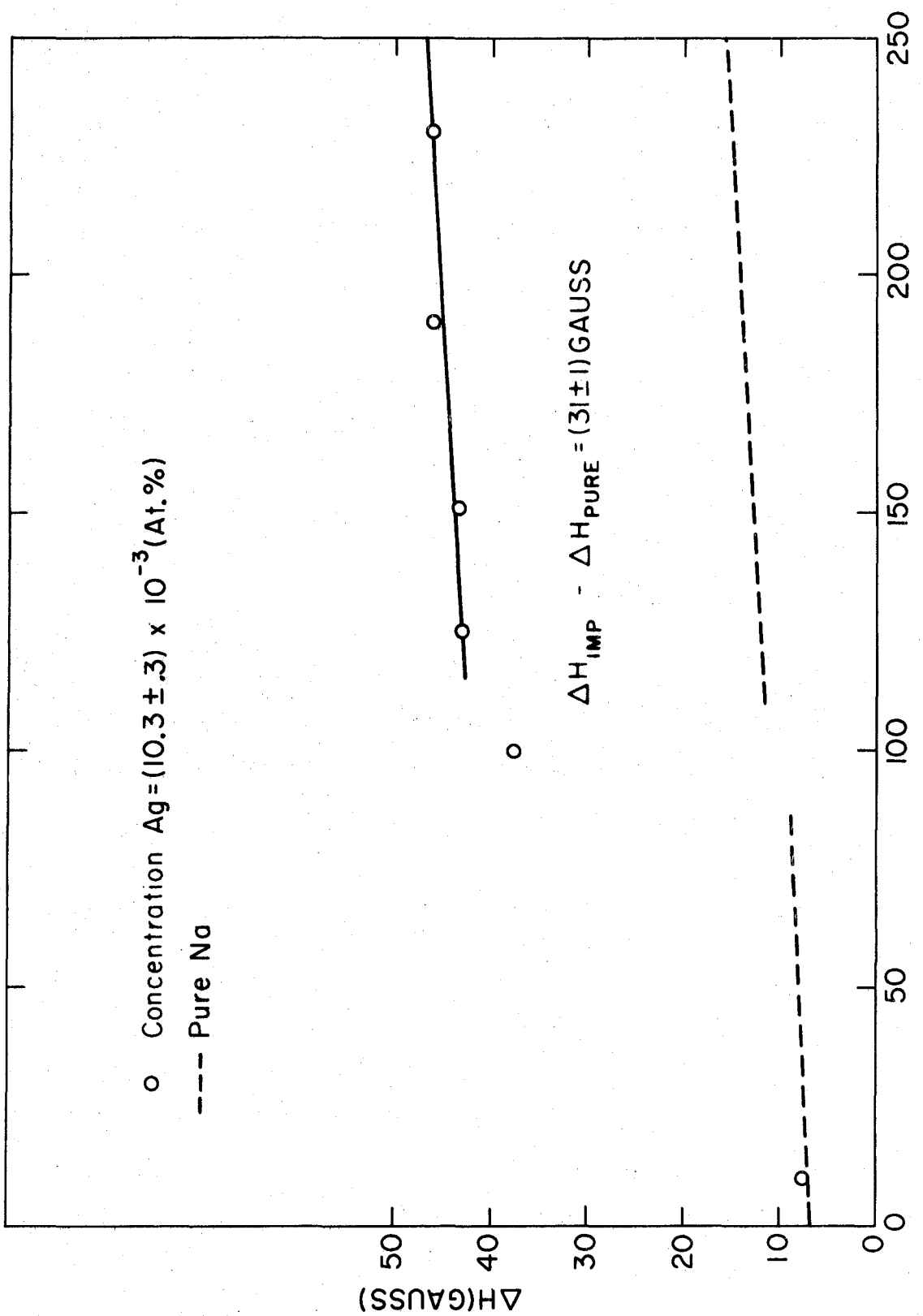
o Concentration Ag=(10.3±.3) x 10^{-3}(At.%)
--- Pure Na
$\Delta H_{IMP} - \Delta H_{PURE} = (31 \pm 1)$ GAUSS
ΔH(GAUSS)
0
10
20
30
40
50
0
50
100
150
200
250
TEMPERATURE(°C)

Figure 10. The temperature dependence of the CESR linewidth of sodium doped with $(20.9 \pm .5) \times 10^{-3}$ at. % silver.

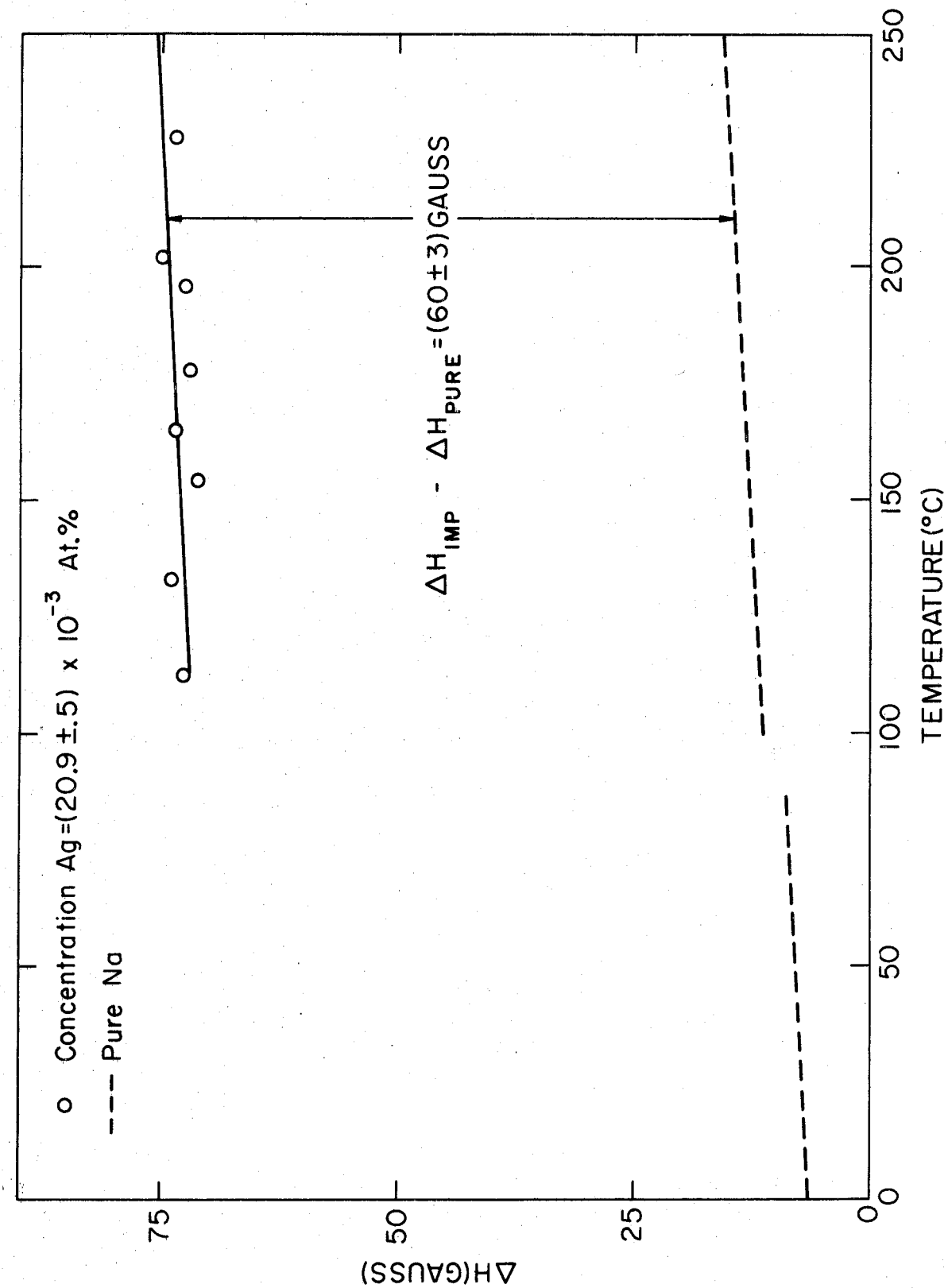
o Concentration Ag=(20.9±.5) x 10⁻³ At.%
--- Pure Na
ΔH_IMP - ΔH_PURE=(60±3)GAUSS
ΔH(GAUSS)
TEMPERATURE(°C)
0
25
50
75
0
50
100
150
200
250

Figure 11. The temperature dependence of the CESR linewidth of sodium doped with $(31.1 \pm 1) \times 10^{-3}$ at. % silver.

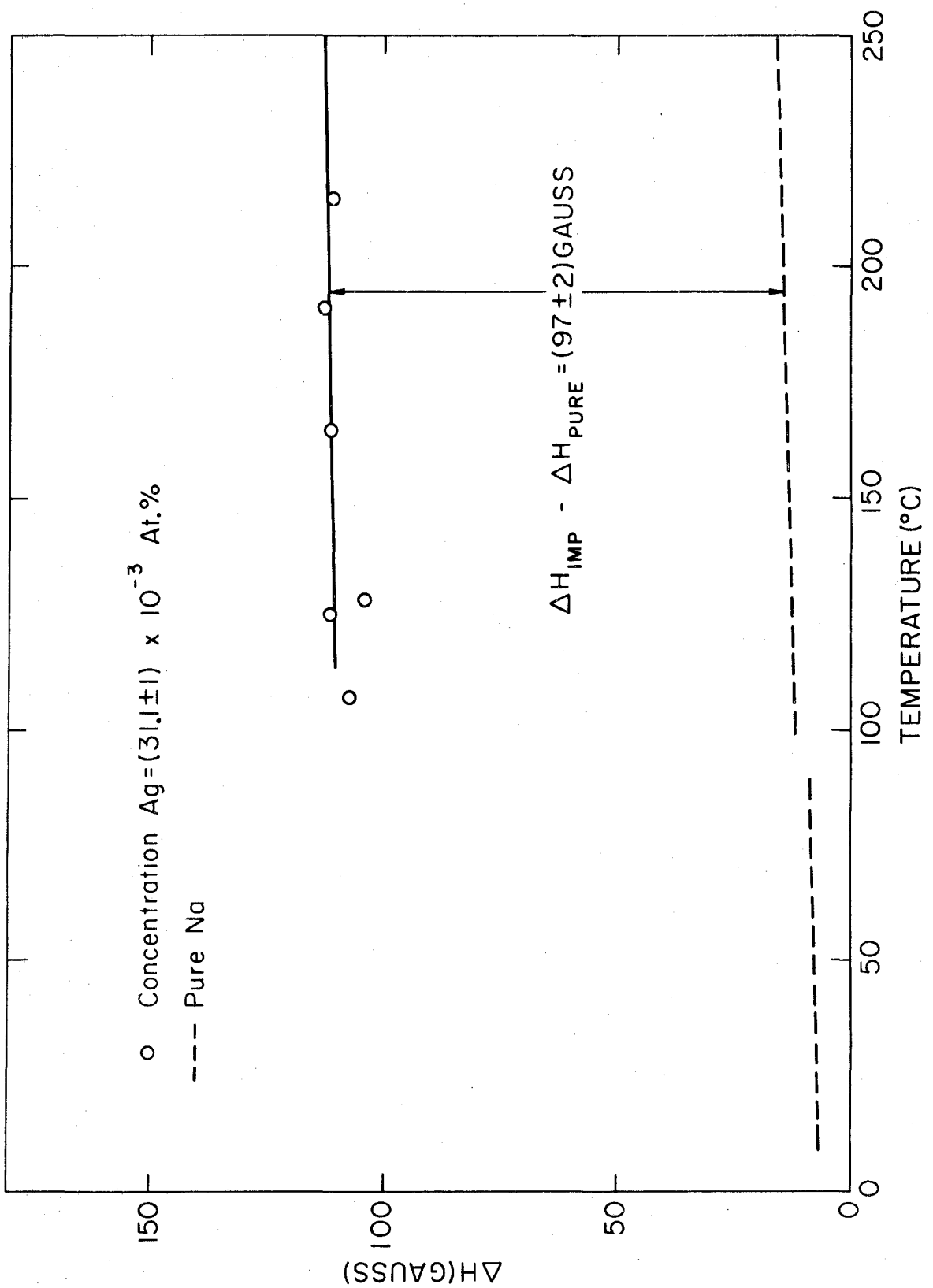
ΔH(GAUSS)
150
100
50
0
0
50
100
150
200
250
TEMPERATURE (°C)
o Concentration Ag=(31.1±1) x 10⁻³ At.%
--- Pure Na
ΔH_IMP - ΔH_PURE = (97±2)GAUSS

continues to increase above T_m with the same slope as pure sodium. The magnitude of the discontinuous jump is directly proportional to the concentration of the impurity involved.

For samples containing bismuth (see Figures 12 to 16), the discontinuity is 2.8 gauss, the same as pure sodium. However, above T_m the linewidth increases more rapidly than pure sodium. This rapid increase continues up to a certain temperature at which point a slope equal to that of pure sodium is assumed. The temperature at which this change in slope occurs depends on the concentration of bismuth.

A third type of behavior, exhibited by palladium-doped sodium samples (see Figures 17 to 20), seems to be a combination of the characteristics exhibited by the other impurities. Samples with concentrations of palladium less than 4.6×10^{-2} at. % behave similarly to platinum- and silver-doped samples, i.e. a discontinuous jump at T_m with the same slope as pure Na above T_m. Samples with concentrations greater than this exhibit discontinuous jumps of 35 gauss at T_m. Above T_m these samples behave similarly to the bismuth-doped samples. A rapid increase of linewidth continues up to a point at which the pure Na slope is assumed. This point depends upon the concentration of paladium. It should be noted that the temperature variation over a sample is about 10°C. Therefore, any sharp discontinuity in ΔH versus temperature curves is rounded over this range.

The fourteen other impurities tested that produced no measurable effects at temperatures up to 300°C are Co, Ni, Cu, Ru, Zn, Ta, Sb, Te, Cr, Mo, Al, Gd, Eu, and Mn.

Figure 12. The temperature dependence of the CESR linewidth of sodium doped with $(4.5 \pm .5) \times 10^{-4}$ at. % bismuth.

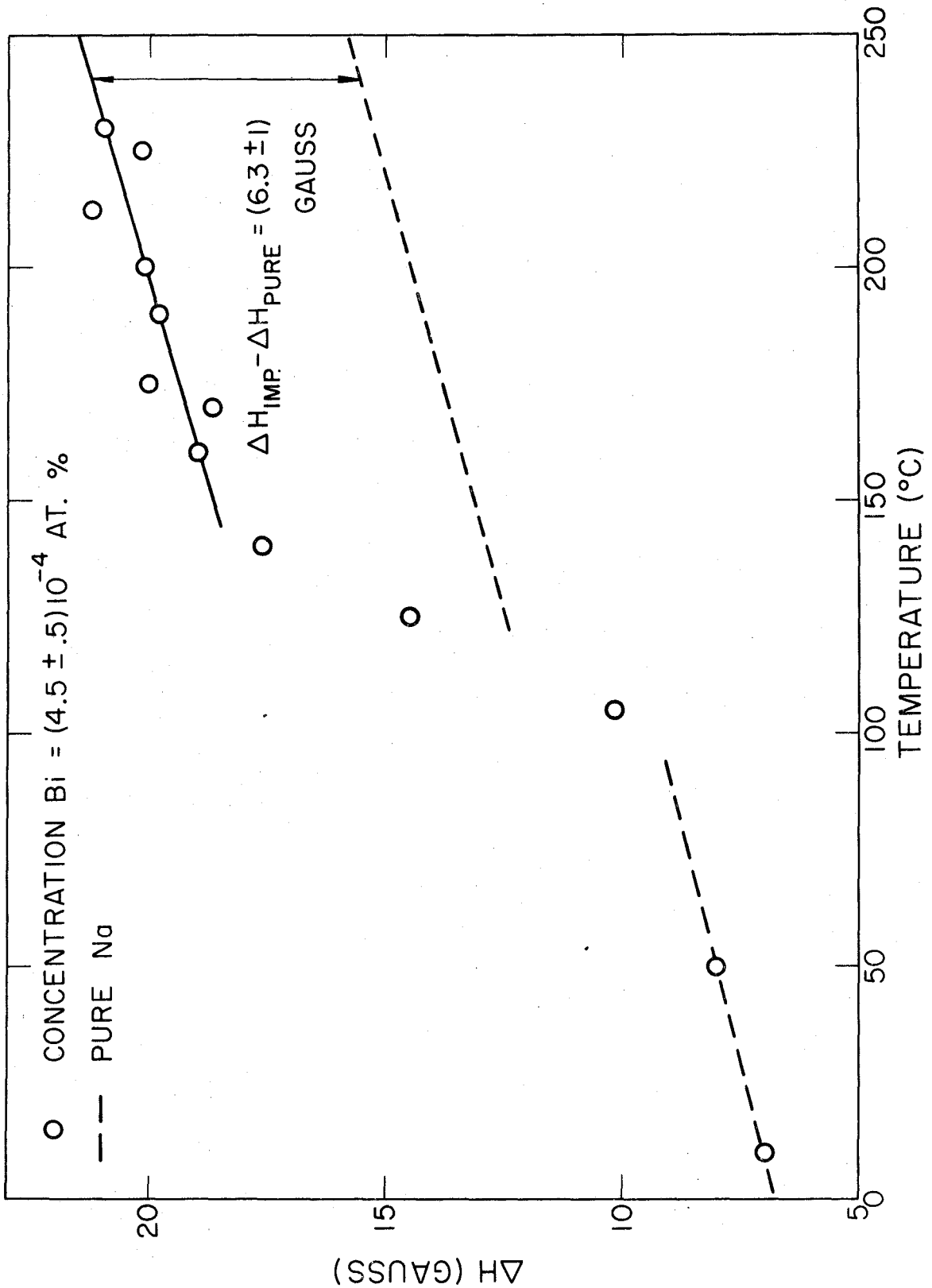
CONCENTRATION Bi = (4.5 ± .5)10^{-4} AT. %
PURE Na
$\Delta H_{IMP.} - \Delta H_{PURE} = (6.3 \pm 1)$ GAUSS
ΔH (GAUSS)
TEMPERATURE (°C)
20
15
10
5
50
100
150
200
250

Figure 13. The temperature dependence of the CESR linewidth of sodium doped with $(6.4 \pm .1) \times 10^{-4}$ at. % bismuth.

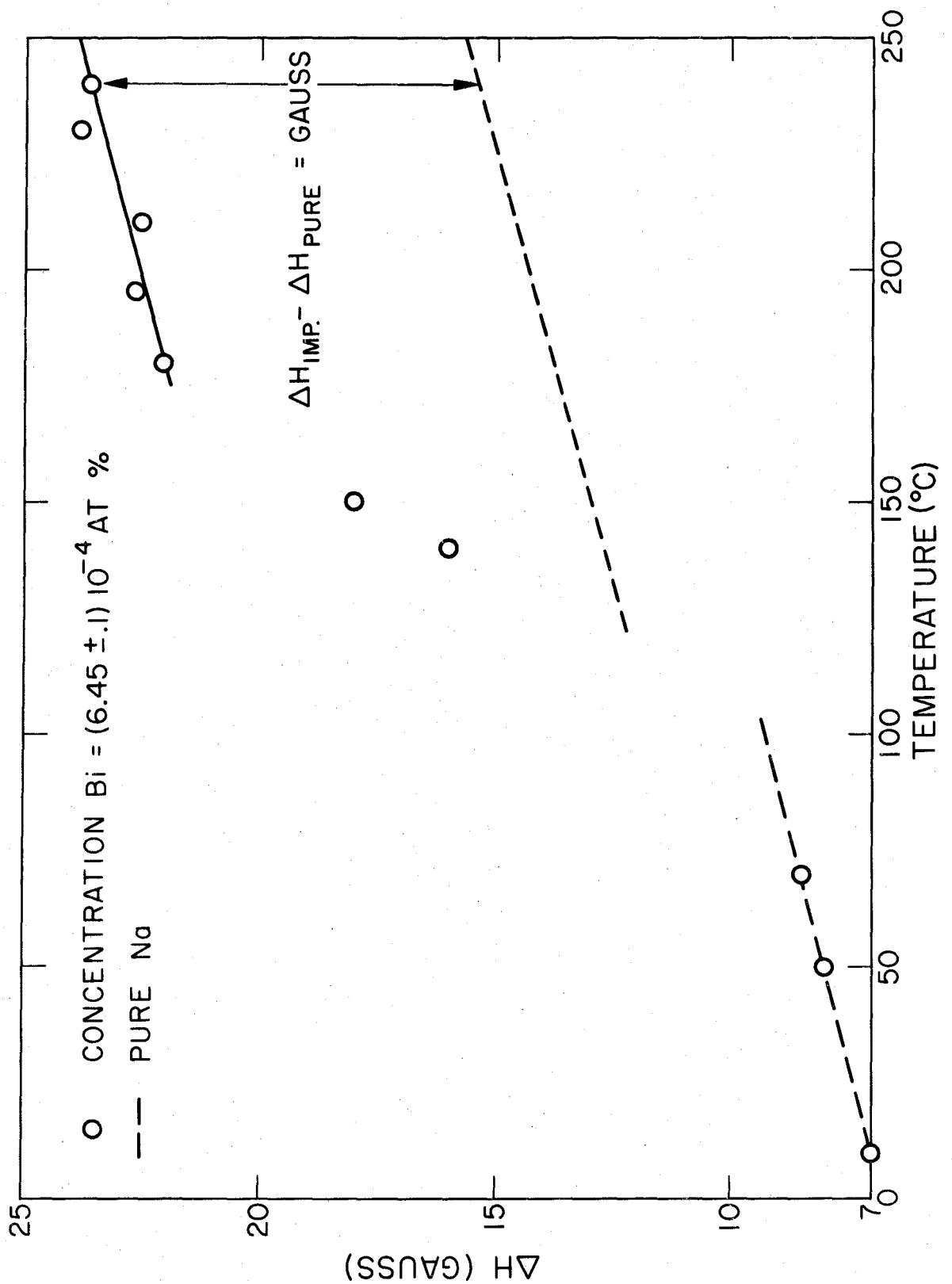
ΔH (GAUSS)
25
20
15
10
7
0
50
100
150
200
250
TEMPERATURE (°C)
O CONCENTRATION Bi = (6.45 ± .1) 10^{-4} AT %
PURE Na
$\Delta H_{IMP.} - \Delta H_{PURE}$ = GAUSS

Figure 14. The temperature dependence of the CESR linewidth of sodium doped with $(9.9 \pm .3) \times 10^{-4}$ at. % bismuth.

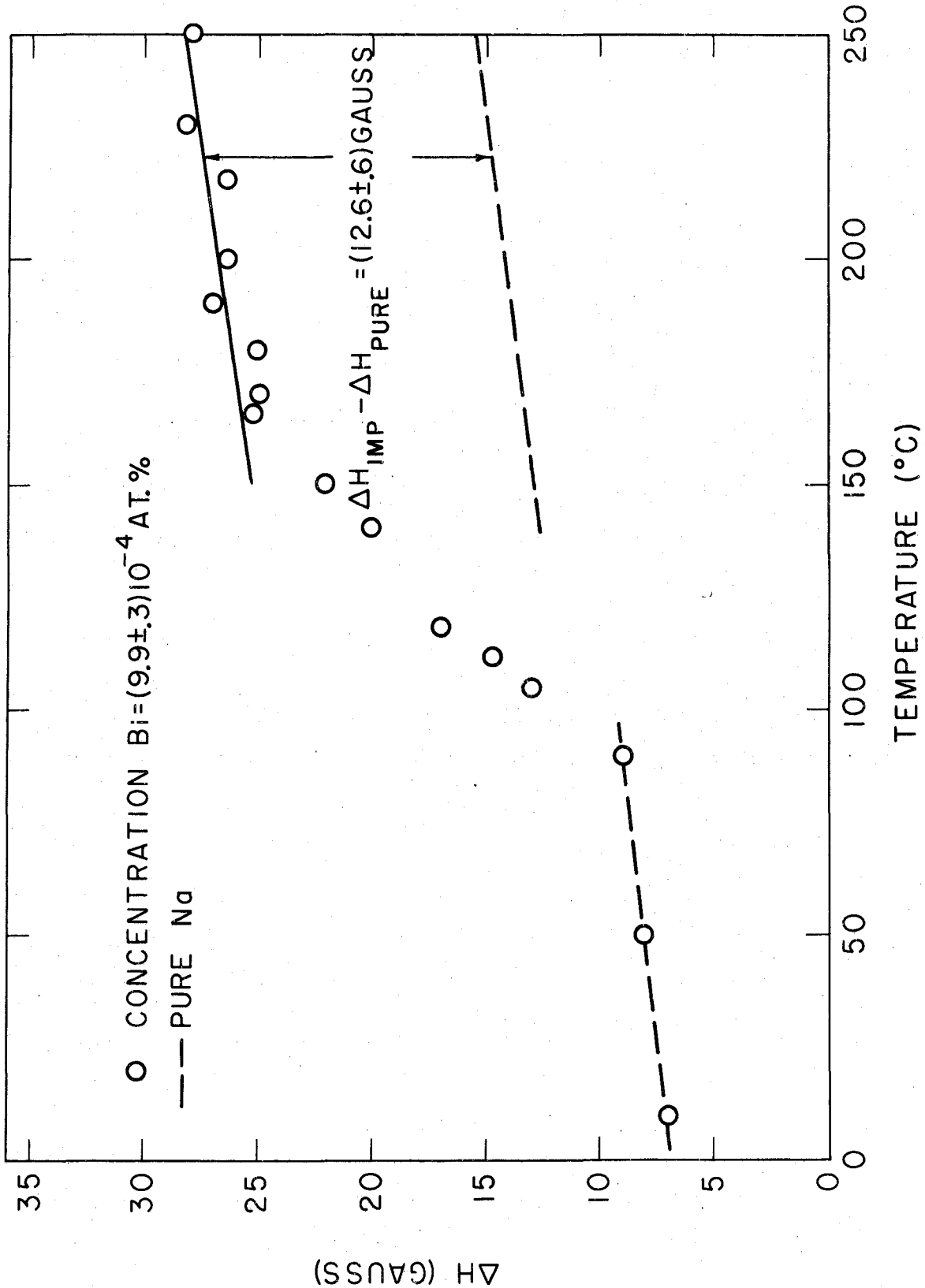
O CONCENTRATION Bi=(9.9±.3)10⁻⁴ AT.%
— — PURE Na
O ΔH_IMP − ΔH_PURE = (12.6±.6) GAUSS
ΔH (GAUSS)
TEMPERATURE (°C)
0
5
10
15
20
25
30
35
0
50
100
150
200
250

Figure 15. The temperature dependence of the CESR linewidth of sodium doped with $(13.1 \pm .5) \times 10^{-4}$ at. % bismuth.

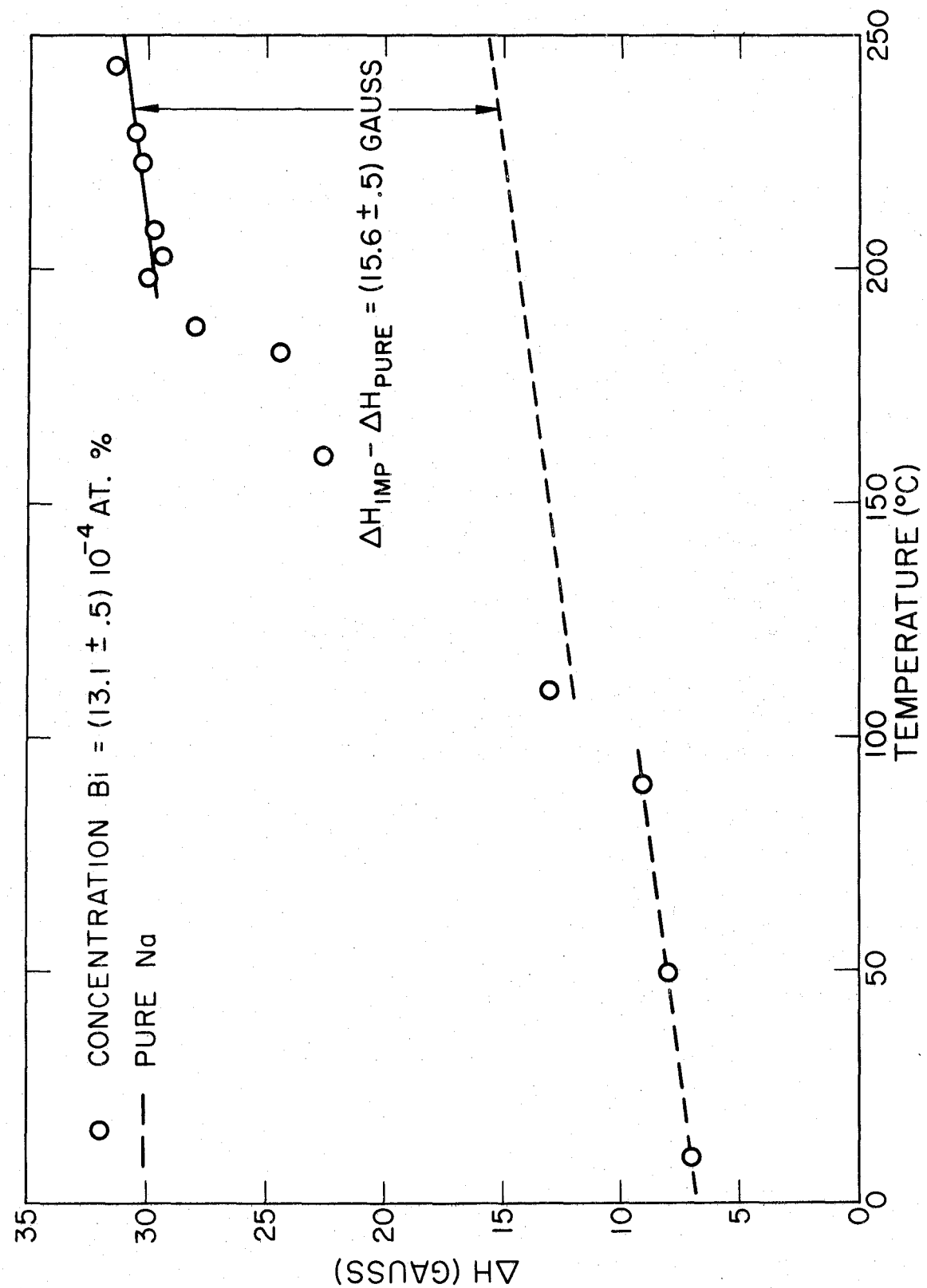
O CONCENTRATION Bi = (13.1 ± .5) 10^{-4} AT. %
PURE Na
$\Delta H_{IMP} - \Delta H_{PURE}$ = (15.6 ± .5) GAUSS
ΔH (GAUSS)
TEMPERATURE (°C)
0
5
10
15
20
25
30
35
50
100
150
200
250

Figure 16. The temperature dependence of the CESR linewidth of sodium doped with large concentrations of bismuth.

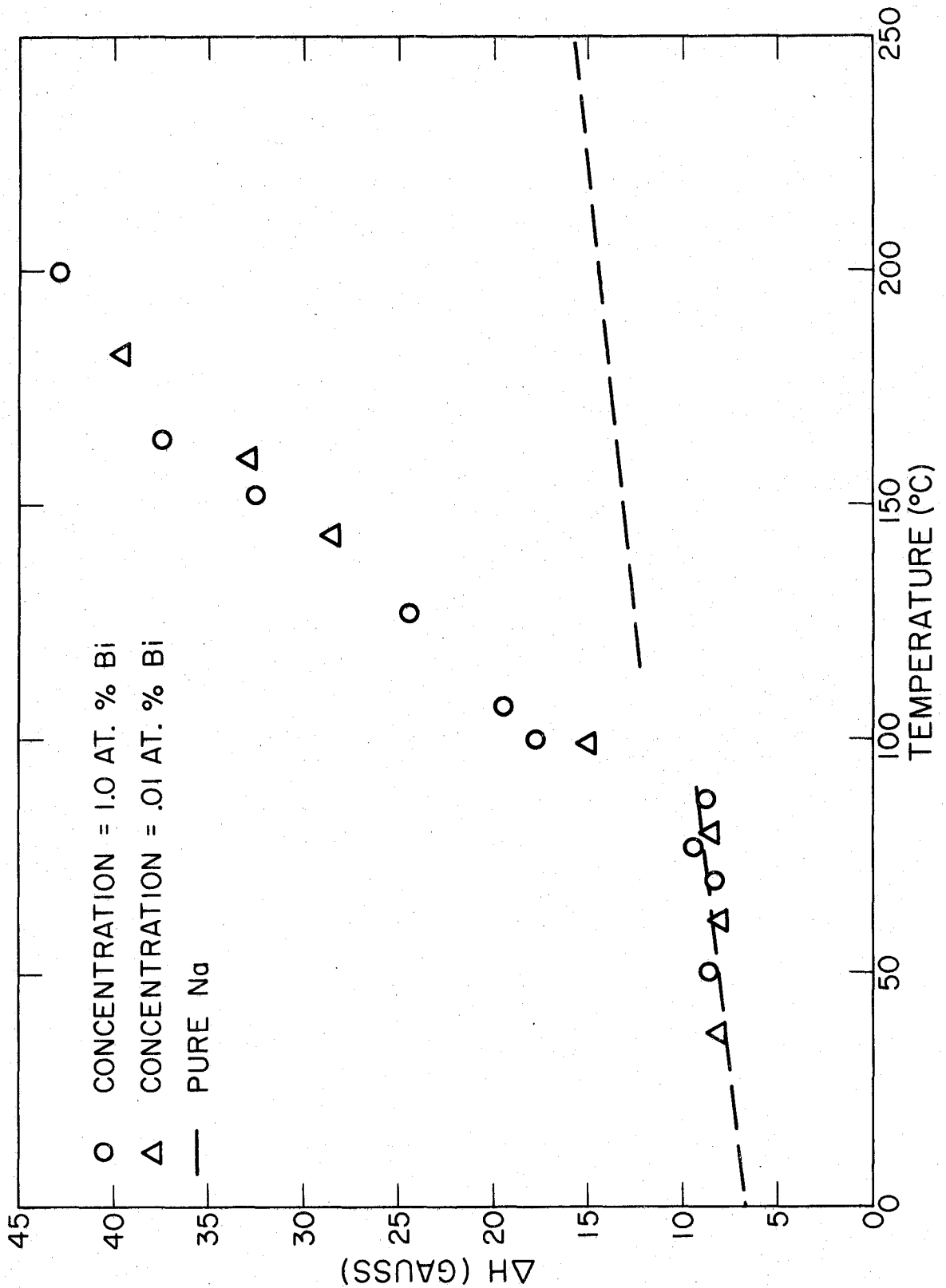
O CONCENTRATION = 1.0 AT. % Bi
Δ CONCENTRATION = .01 AT. % Bi
PURE Na
ΔH (GAUSS)
TEMPERATURE (°C)
0
5
10
15
20
25
30
35
40
45
50
100
150
200
250

Figure 17. The temperature dependence of the CESR linewidth of sodium doped with 1.13×10^{-2} at. % palladium.

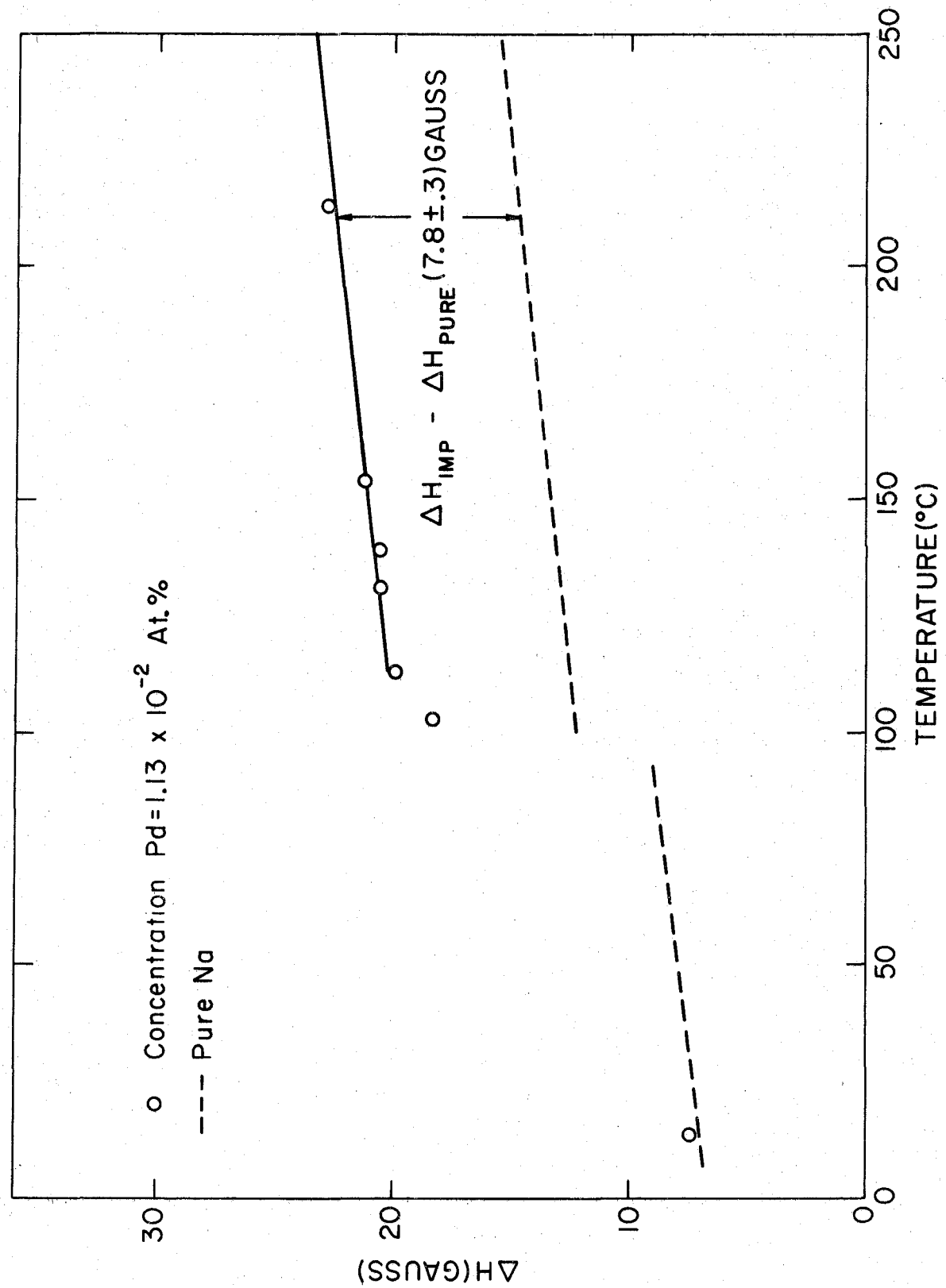
o Concentration Pd=1.13 x 10⁻² At.%
--- Pure Na
ΔH_IMP - ΔH_PURE (7.8±.3) GAUSS
ΔH (GAUSS)
TEMPERATURE (°C)
0
10
20
30
50
100
150
200
250

Figure 18. The temperature dependence of the CESR linewidth of sodium doped with 2.75×10^{-2} at. % palladium.

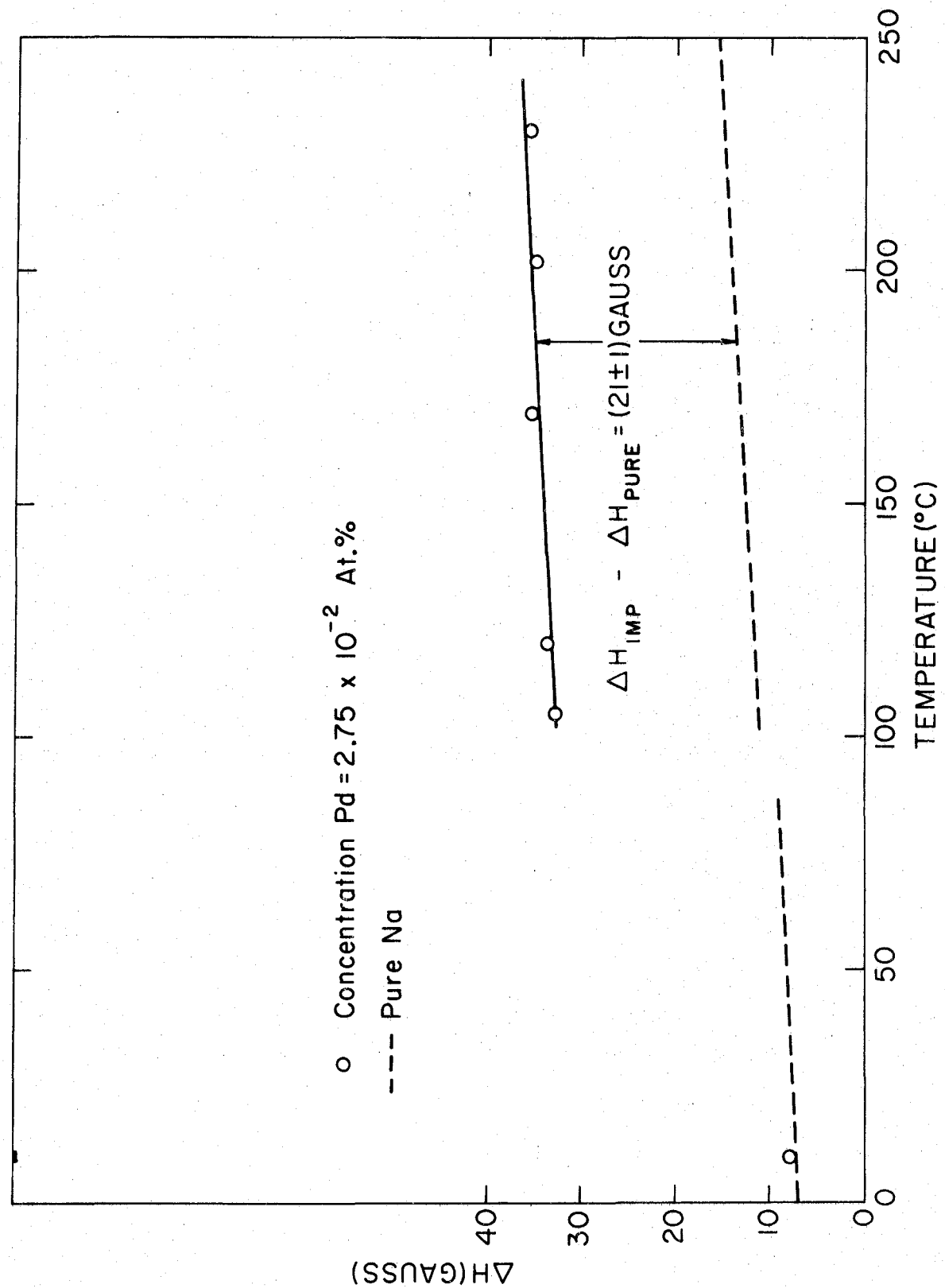
o Concentration Pd = 2.75 x 10⁻² At.%
--- Pure Na
ΔH_IMP - ΔH_PURE = (21±1) GAUSS
ΔH (GAUSS)
TEMPERATURE (°C)
0
10
20
30
40
0
50
100
150
200
250

Figure 19. The temperature dependence of the CESR linewidth of sodium doped with 5.6×10^{-2} at. % palladium.

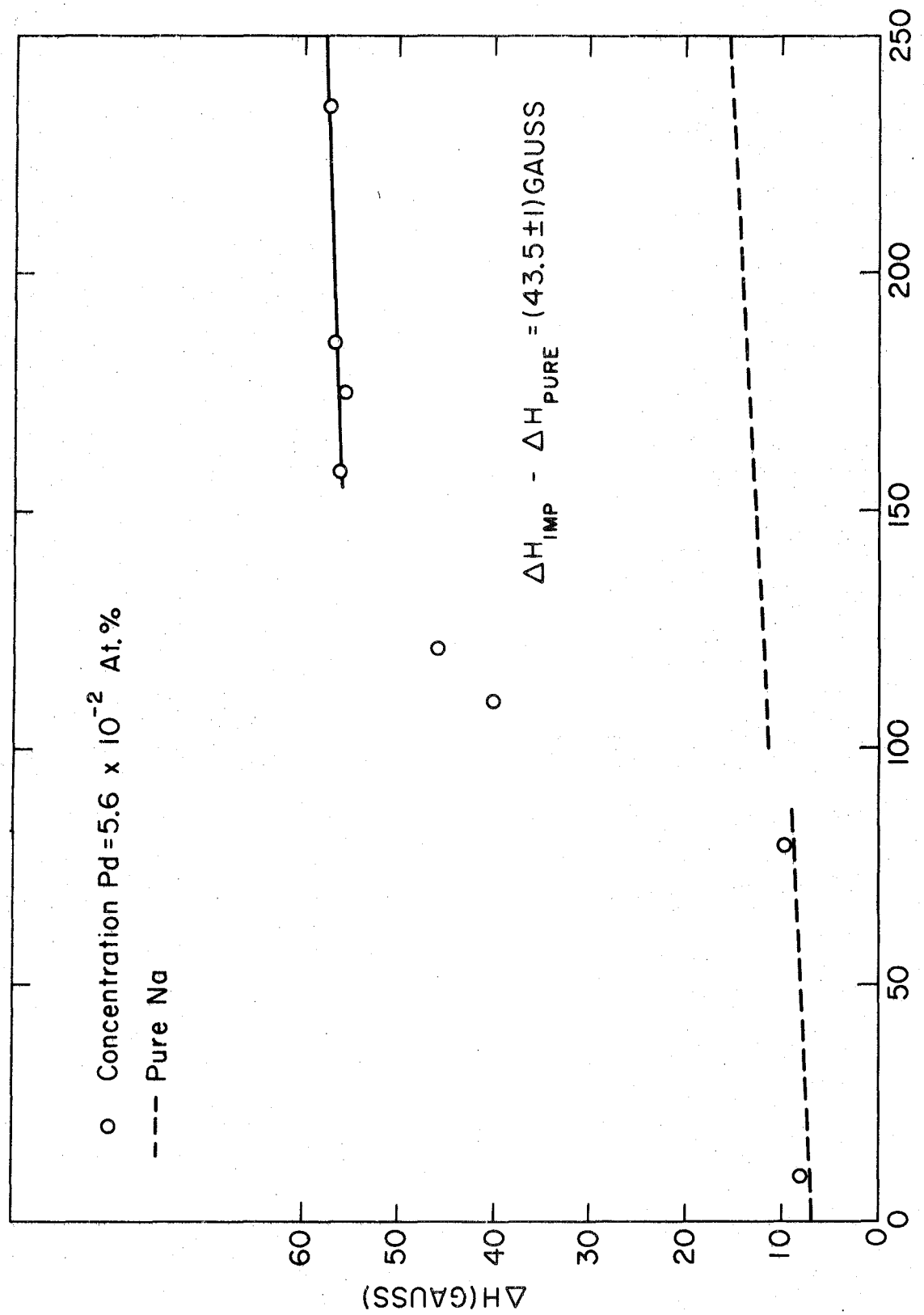
o Concentration Pd=5.6 x 10^{-2} At.%
--- Pure Na
$\Delta H_{IMP} - \Delta H_{PURE} = (43.5 \pm 1)$GAUSS
ΔH(GAUSS)
TEMPERATURE(°C)
0
10
20
30
40
50
60
0
50
100
150
200
250

Figure 20. The temperature dependence of the CESR linewidth of sodium doped with large concentrations of palladium.

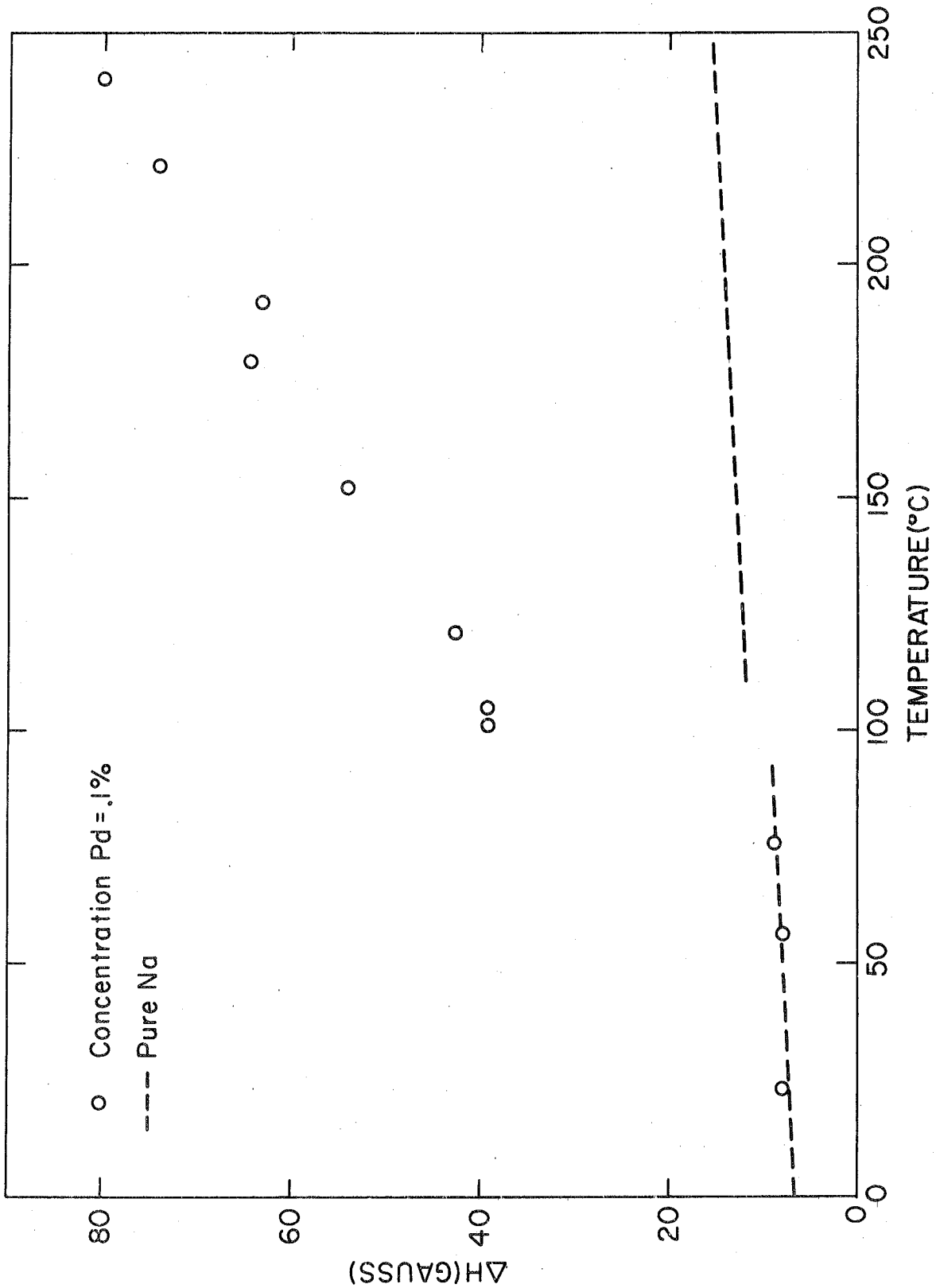
ΔH(GAUSS)
0
20
40
60
80
0
50
100
150
200
250
TEMPERATURE(°C)
o Concentration Pd = .1%
--- Pure Na

B. Experimental Results in Terms of Solubility Curves

The three types of behavior of the CESR linewidth as a function of temperature can be explained easily by accounting for the solubility of the impurities. Upon melting, sodium is capable of dissolving a relatively large amount of platinum and silver. Thus, at T_m the jump in linewidth corresponds to the broadening produced by the dissolution of all the impurity available. The change in this jump is a direct measure of the broadening factor of these impurities. Above T_m no more impurity can dissolve, so any change in linewidth with temperature is due only to the properties of the host metal. Hence a pure sodium slope is assumed.

The other two types of behavior are exhibited by bismuth and palladium. The equilibrium dissolved concentrations of palladium and bismuth as a function of temperature are shown in Figures 21 and 22 respectively. Those figures were obtained by first determining the broadening factors (see the next section) for the two impurities and then applying this factor to Figures 39 and 43.

For bismuth (Figure 22) in the range of concentrations which produce measurable linewidth broadening, the amount dissolved depends upon temperature. Just at T_m, very little impurity is dissolved. Hence no increase in the discontinuity results from impurity broadening. As the temperature increases, more and more impurity goes into solution and the resulting impurity-induced broadening increases. This continues until a temperature is reached which will maintain a dissolved concentration that accounts for all the available impurity. Since above this temperature the concentration of dissolved impurity cannot increase, the linewidth

assumes the pure sodium temperature dependence. For larger concentrations this leveling off should occur at higher temperatures.

In the case of palladium (Figure 21) we find that at T_m sodium is capable of dissolving a concentration of 4.6×10^{-2} at. % palladium. Above the melting point, larger concentrations can be dissolved. Thus, a discontinuous jump greater than 2.8 gauss occurs at T_m. If the concentration of palladium is less than 4.6×10^{-2} at. %, all available impurity is dissolved and no further impurity-induced broadening occurs. If the concentration is greater than this, the jump is 35 gauss, and above T_m impurity broadening gives rise to an increasing slope until all available impurity is dissolved.

Theoretically, if larger linewidths could be measured, then large enough concentrations of platinum and silver could be used so that not all the available impurity would dissolve at T_m. Then further impurity-induced broadening would take place above the melting temperature.

Using the conduction electron spin resonance technique, impurity concentrations as low as 10^{-4} at. % can be measured. This is three orders of magnitude more sensitive than other techniques usually used. As a result the existing data in the literature on solubility of low concentrations of impurities in lithium and sodium is meager and a comparison with Figures 21 and 22 is not very meaningful. As an example, note that at 100°C a concentration of .35 at % bismuth is supposed to be soluble in sodium.[33] Figure 22 shows only 5×10^{-4} at. % bismuth soluble at this temperature. No quantitative information on palladium exists.

One logical attack on the problem of calculating solubility curves would be to form a physical model of the system and caculate solubilities.[34]

Figure 21. The temperature dependence of the concentration of palladium dissolved in sodium.

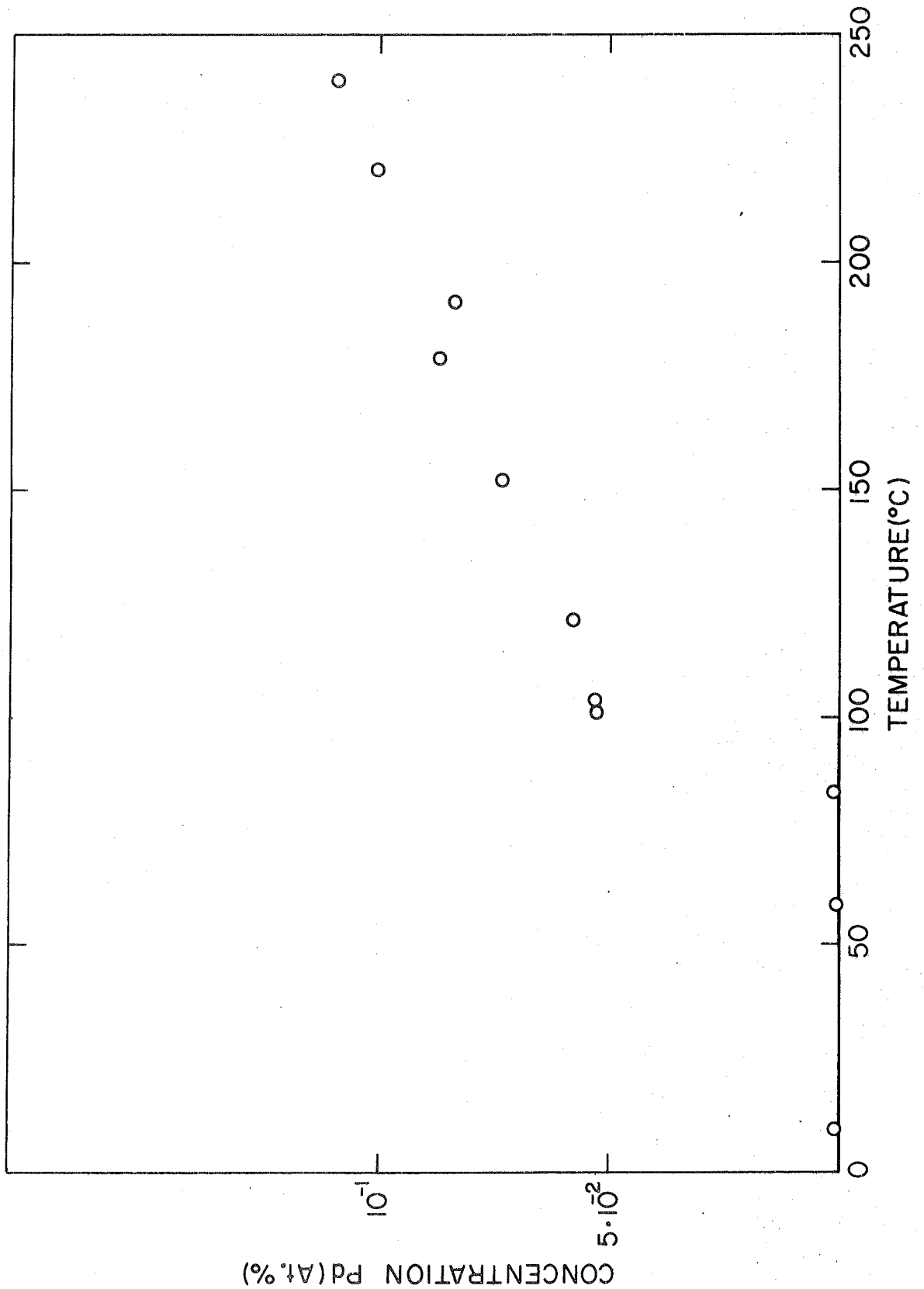
CONCENTRATION Pd(At.%)
10^{-1}
$5 \cdot 10^{-2}$
0
50
100
150
200
250
TEMPERATURE(°C)

Figure 22. The temperature dependence of the concentration of bismuth dissolved in sodium.

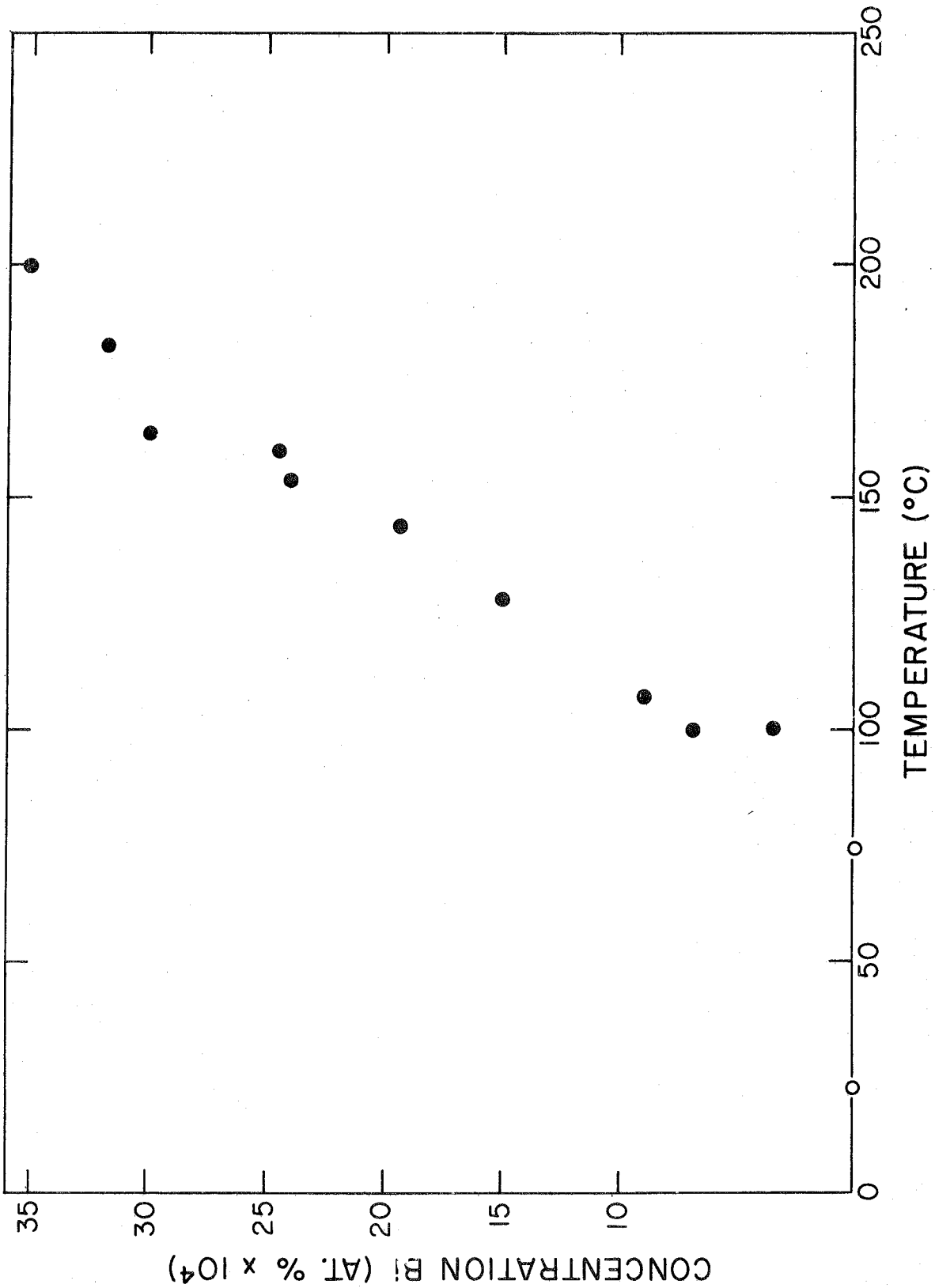
CONCENTRATION Bi (AT. % x 10⁴)
35
30
25
20
15
10
0
50
100
150
200
250
TEMPERATURE (°C)

Though there has been some success in explaining phase boundaries in solid alloys,[33] there has been little headway made in predicting solubilities from first principles.

Another approach to this problem is through thermodynamical considerations. As was stated above, a direct comparison between the data obtained from electron spin resonance experiments with results from other techniques is not feasable. However the low concentration regions can be used to find the change in entropy and enthalpy when an impurity atom is dissolved. These can be compared with values obtained at higher concentrations and temperatures. To the extent that the enthalpy and entropy changes are independent of concentration and temperature this is a meaningful comparison. Under the assumption that the impurity concentrations are small enough to let each atom be considered as unaffected by other impurity atoms, it is a general result that concentration can be expressed by

$$C = e^{\Delta S/R} \times e^{-\frac{\Delta H}{RT}} , \qquad (8)$$

where ΔS and ΔH are the change in entropy and enthalpy of the system when one mole of solute goes into solution. Nowick and Freedman[34] have applied equation (8) to 21 different binary systems and thus determined the entropy and enthalpy of solution. Figures 23 and 24 show a plot of log(1/c) against 1/T for the palladium and bismuth data resulting from the present experiment. The calculations of ΔS and ΔH are given in Table II. Seith and Kuascshewskie,[35] using calorimetric techniques, have measured ΔH for bismuth in sodium in the concentration range of 5% to 25%. They found ΔH to be independent of concentration and equal to

Figure 23. Log (1/c) vs 1/T for bismuth in sodium.

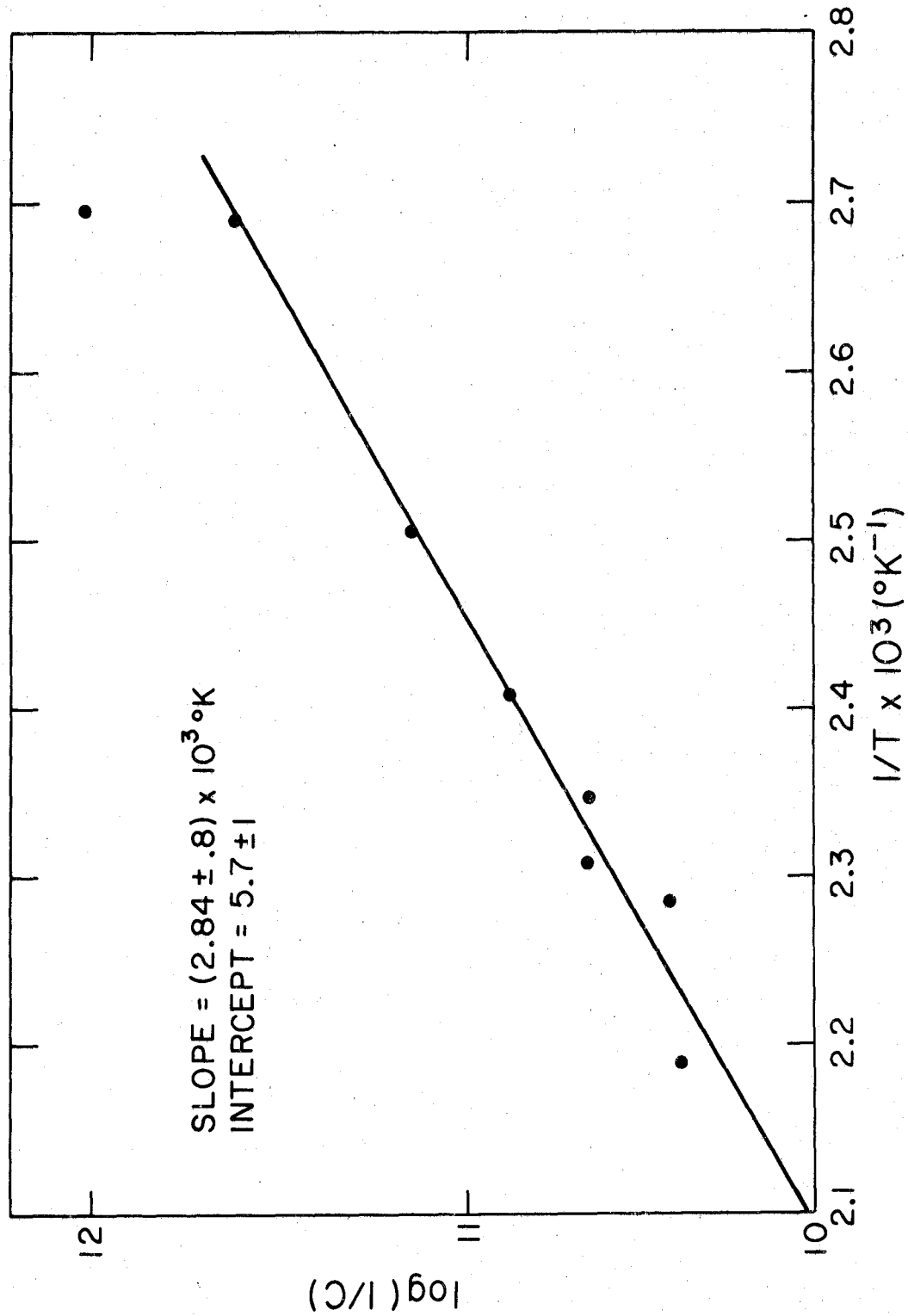
log (1/C)
12
11
10
2.1
2.2
2.3
2.4
2.5
2.6
2.7
2.8
1/T x 10³ (°K⁻¹)
SLOPE = (2.84 ± .8) x 10³ °K
INTERCEPT = 5.7 ± 1

Figure 24. Log(1/c) vs 1/T for palladium in sodium.

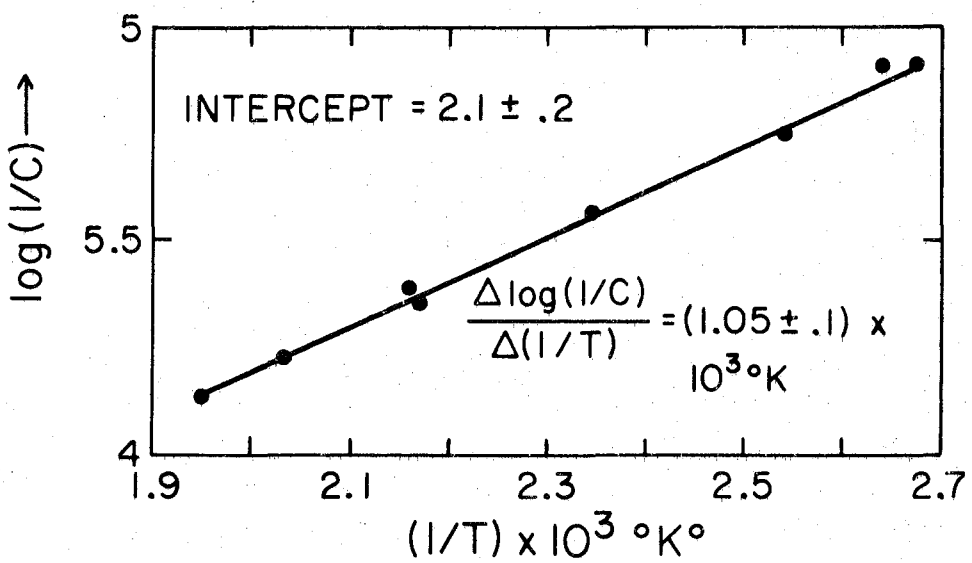
5
5.5
4
log (1/C) ⟶
INTERCEPT = 2.1 ± .2
Δ log (1/C) / Δ (1/T) = (1.05 ± .1) x 10³ °K
1.9
2.1
2.3
2.5
2.7
(1/T) x 10³ °K°

Table II

Entropy and Enthalpy of Solution as Determined from Solubility Curves

Solute	△H(k cal/mole)	△S(cal/mole°K)
Bismuth	5.7 ± 1.6	10.4
Palladium	2.1 ± 0.2	9.2

11.4 ± 1 kcal/mole. When the different ranges of concentrations are considered, this is comparable to the value of 5.7 ± 1.6 shown in Table II. Actually it is somewhat surprising that Seith and Kubaschewski found ΔH to be independent of concentration for concentrations as high as 25% where interactions between impurity atoms are bound to enter in.

Figures 25 and 26 summarize the ability of sodium and lithium to form dilute disordered alloys. If relative atomic size is considered, it seems reasonable that sodium should not form alloys as easily as lithium. The atomic radius of sodium. 1.9 Å differs at most by 11%. Home-Rothery found in an empirical study of alloys that the effect of an unfavorable size factor seems to come into play rather suddenly when atomic radii differ by about 15%.[36]

C. Experimental Results in Terms of Scattering Cross Sections

The broadening factor $\frac{\partial \Delta H}{\partial C}$ is obtained by measuring the vertical displacement $(\Delta H_{imp} - \Delta H_{pure})$ of the impurity doped linewidth curve from that of pure sodium. This is done at the high temperature end to ensure that all the impurity is dissolved. Then $\Delta H_{imp} - \Delta H_{pure}$ is plotted against concentration, the slope being the broadening factor $\frac{\partial \Delta H}{\partial C}$ (see Figures 27-30).

This broadening factor can be related to the spin-flip scattering cross section of the impurity atom. First consider the CESR lineshape. When particle sizes are less than the skin depth δ, CESR lineshapes are lorentzian. For measurements made in the microwave region (10 kmc/sec) the particle sizes are larger than δ (which is 1 micron for Na at 300°C and X-band). Thus one has to take into account diffusion of the conduction electron into and out of the range of the magnetic fields at

Figure 25. The ability of impurities to dissolve in lithium arranged as in the periodic table.

N NOT SOLUBLE IN SOLID LITHIUM

P SOLUBLE IN SOLID LITHIUM UP TO FINITE CONCENTRATION

S SOLUBLE IN SOLID LITHIUM

* IMPURITY PRECIPITATED OUT OF SOLUTION AFTER FEW DAYS

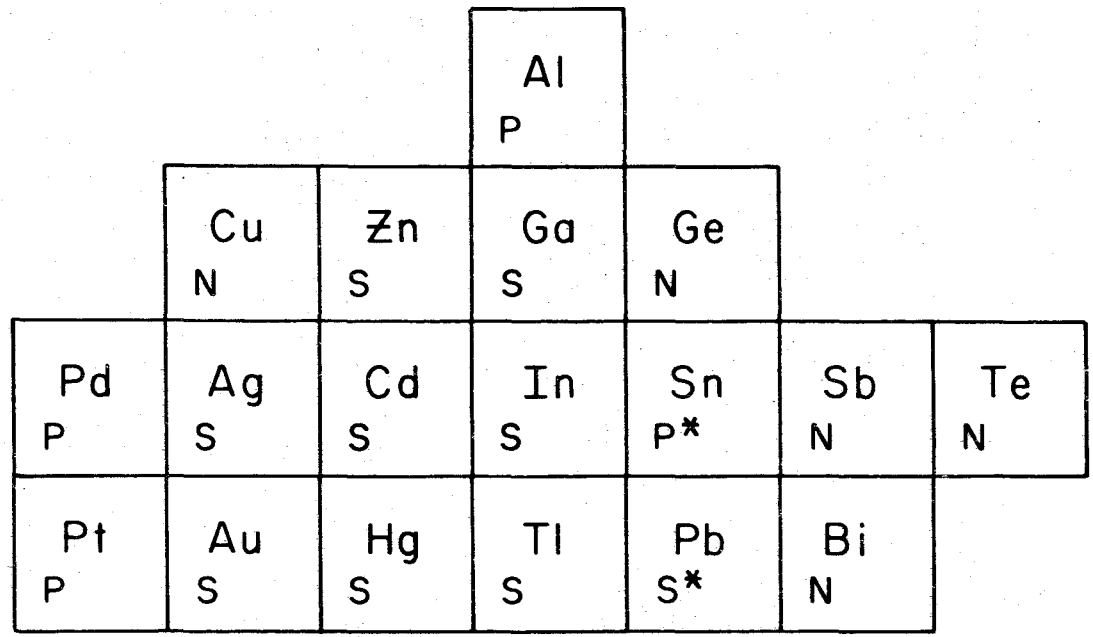

Figure 26. The ability of impurities to dissolve in sodium arranged as in the periodic table.

S SOLUBLE IN SOLID SODIUM

N NOT SOLUBLE IN SODIUM

M SOLUBLE IN LIQUID SODIUM ONLY

P SOLUBLE IN SOLID SODIUM UP TO A FINITE CONCENTRATION

			Al N			
	Cu N	Zn N	Ga N	Ge N		
Pd M	Ag M	Cd S	In S	Sn P M	Sb N	Te N
Pt M	Au S	Hg S	Tl S	Pb S	Gi M	

Figure 27. The dependence of the CESR linewidth on concentration for NaBi alloys.

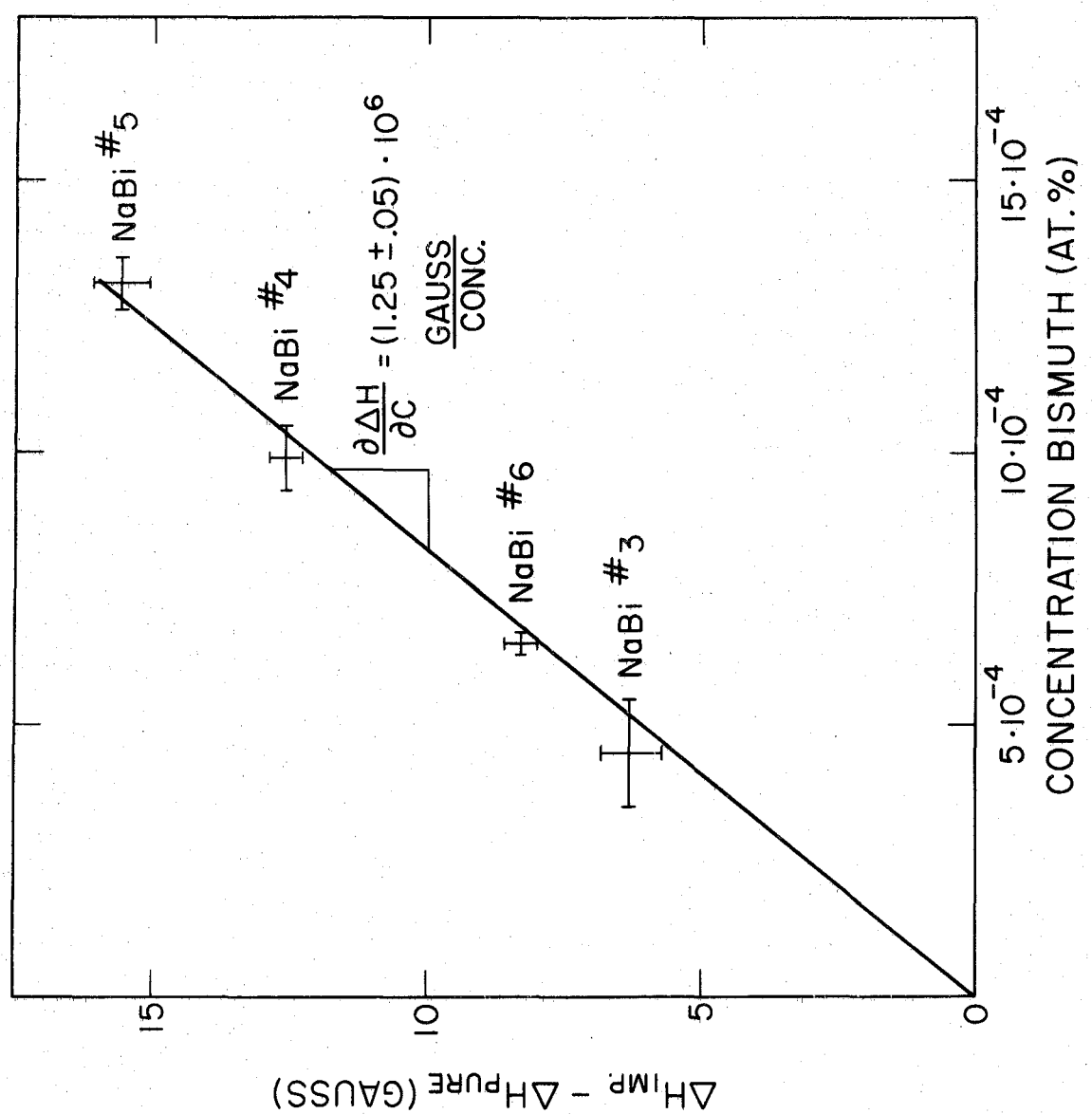
NaBi #5
NaBi #4
NaBi #6
NaBi #3
$\frac{\partial \Delta H}{\partial C} = (1.25 \pm .05) \cdot 10^6 \frac{\text{GAUSS}}{\text{CONC.}}$
$\Delta H_{IMP} - \Delta H_{PURE}$ (GAUSS)
0
5
10
15
$5 \cdot 10^{-4}$
$10 \cdot 10^{-4}$
$15 \cdot 10^{-4}$
CONCENTRATION BISMUTH (AT.%)

Figure 28. The dependence of the CESR linewidth on concentration for NaPt alloys.

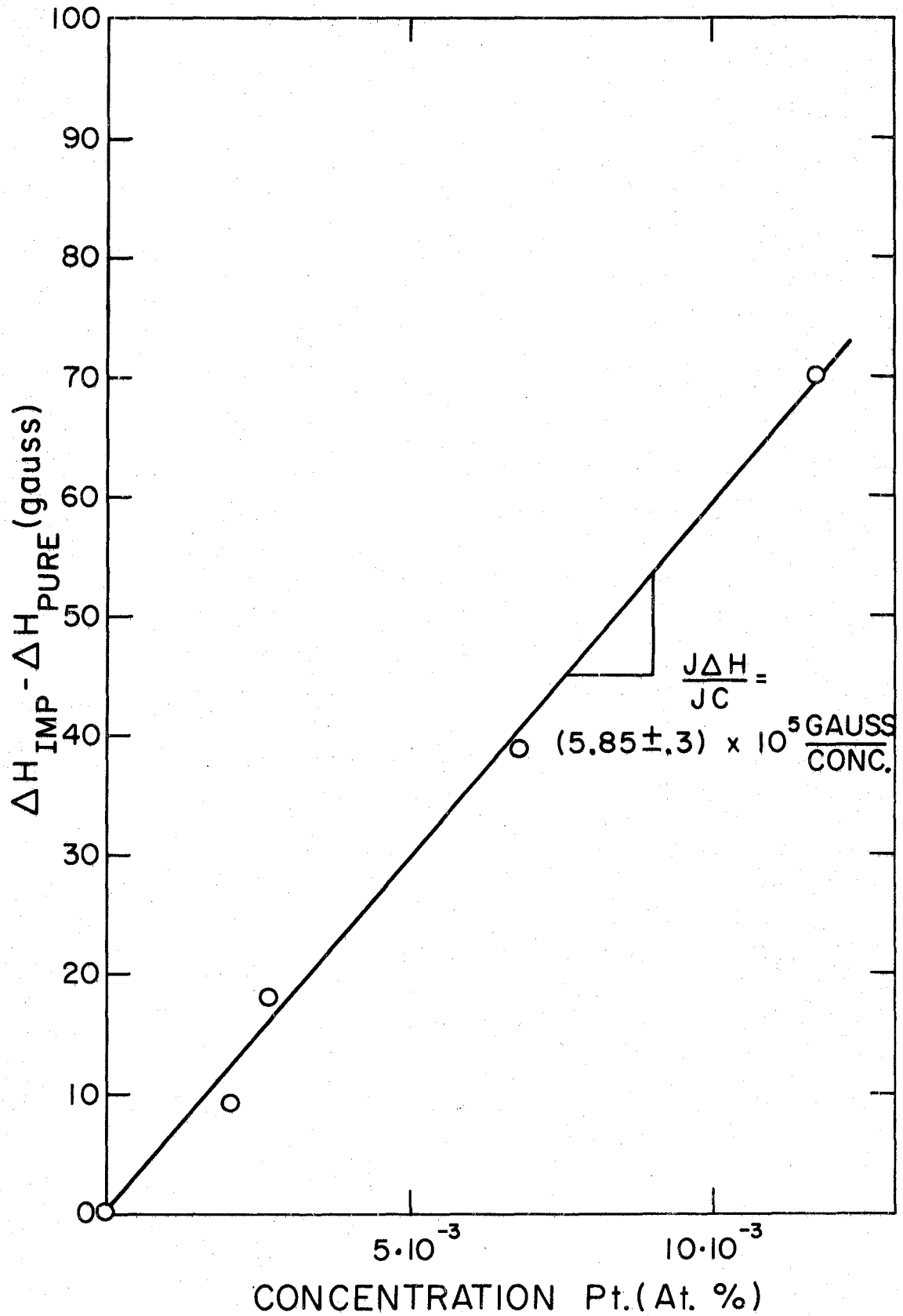
100
90
80
70
60
50
40
30
20
10
0
$\Delta H_{IMP} - \Delta H_{PURE}$ (gauss)
$\frac{J\Delta H}{JC} =$
$(5.85 \pm .3) \times 10^5 \frac{\text{GAUSS}}{\text{CONC.}}$
$5 \cdot 10^{-3}$
$10 \cdot 10^{-3}$
CONCENTRATION Pt. (At. %)

Figure 29. The dependence of the CESR linewidth on concentration for NaPd alloys.

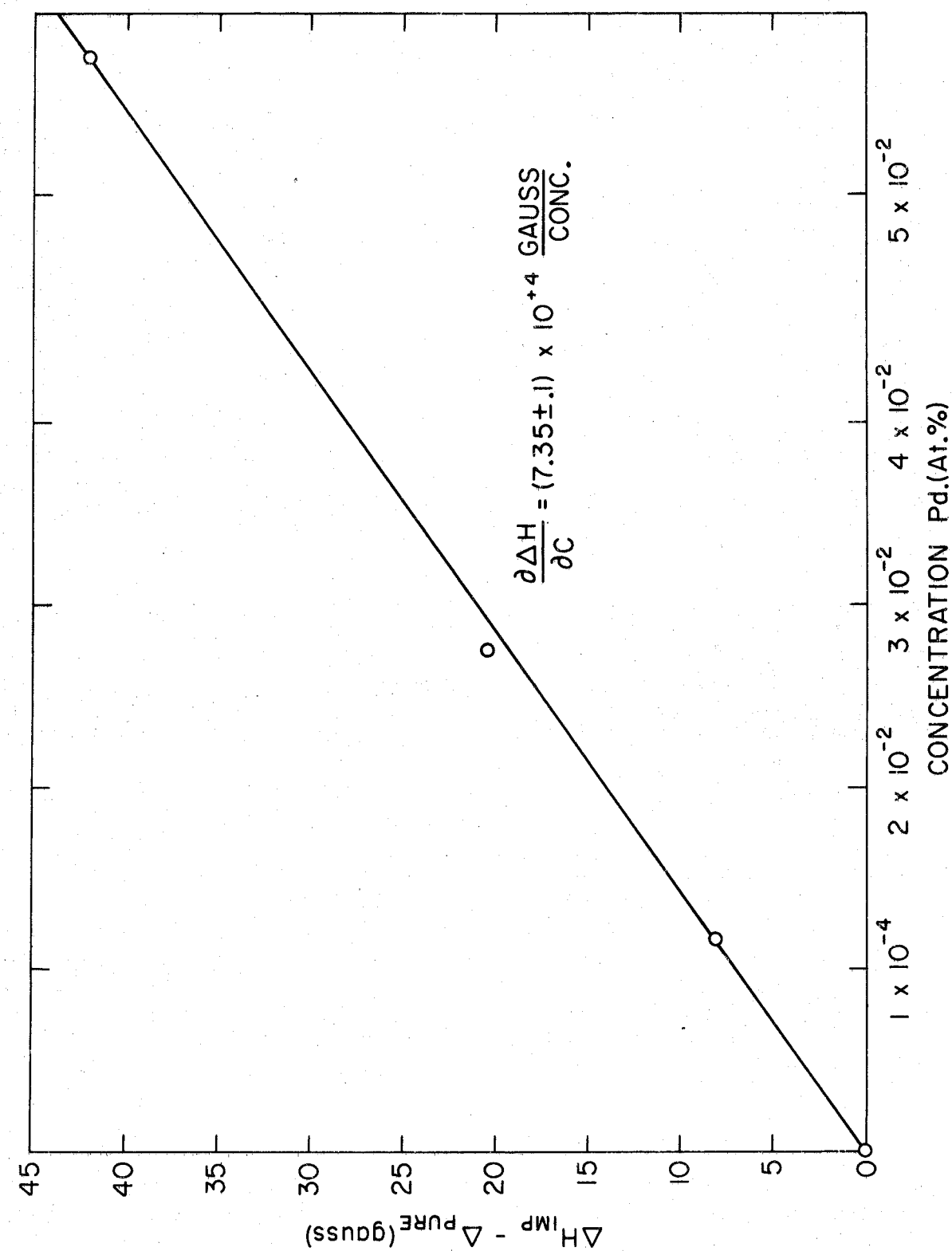
$\frac{\partial \Delta H}{\partial C} = (7.35 \pm .1) \times 10^{+4} \frac{\text{GAUSS}}{\text{CONC.}}$
$\Delta H_{IMP} - \Delta_{PURE}$ (gauss)
0
5
10
15
20
25
30
35
40
45
1×10^{-4}
2×10^{-2}
3×10^{-2}
4×10^{-2}
5×10^{-2}
CONCENTRATION Pd.(At.%)

Figure 30. The dependence of the CESR linewidth on concentration for NaAg alloys.

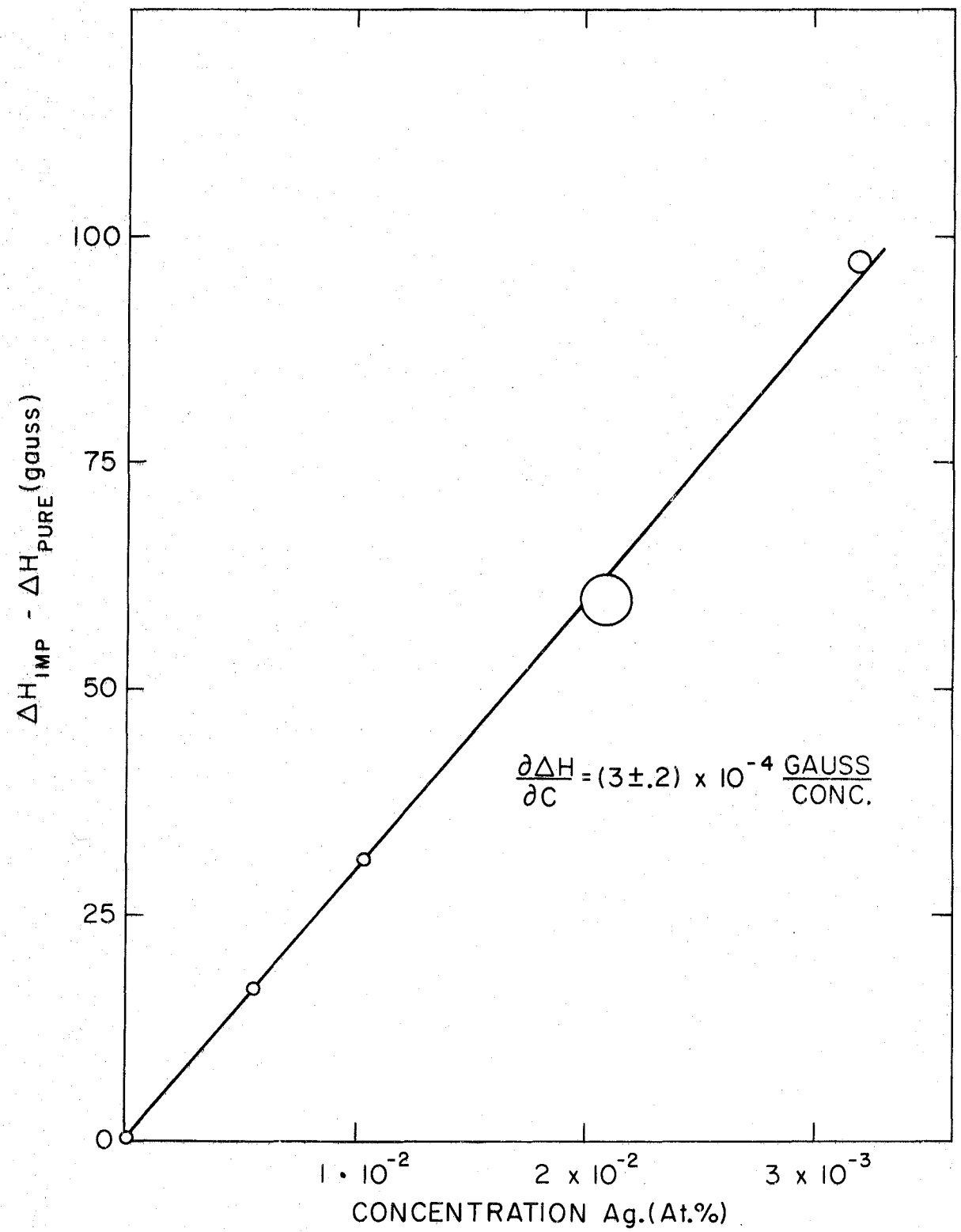
100
75
50
25
0
$\Delta H_{IMP} - \Delta H_{PURE}$ (gauss)
$\frac{\partial \Delta H}{\partial C} = (3 \pm .2) \times 10^{-4} \frac{\text{GAUSS}}{\text{CONC.}}$
$1 \cdot 10^{-2}$
2×10^{-2}
3×10^{-3}
CONCENTRATION Ag.(At.%)

the surface. Dyson[37] has made calculations of the CESR lineshape taking this into account. Applying Dyson's theory to the particle size distributions of sodium and lithium disperions, Asik[10] was able to conclude that

$$\gamma \Delta H T_2 = 1.1 \qquad (9)$$

holds to within ± 10% at worst. Here ΔH is the half height width of the CESR signal, T_2 is the spin-spin relaxation time and γ is the electron gyromagnetic ratio.

We are interested in spin lattice relaxation and since the CESR gives only information about T_2, it is important to know the relationship between T_1, the spin-lattice relaxation time and T_2. Work by Carver and Slichter[38] and Yafet[39] show that it is correct to take T_1 and T_2 to be equal in sodium and lithium. This is a result of the rapid motion of the electron with respect to its larmor frequency and to the isotropic (cubic) lattice structure.

Now let us introduce the concept of spin mean free path ℓs, which is the distance traveled by a conduction electron before its spin is reversed by interaction with an impurity atom. By definition of the scattering cross section we have

$$\ell s = \frac{1}{N_o c \sigma_{sf}} \qquad (10)$$

where N_o is the number of host atoms per cm^3 and c is the fractional concentration of impurity atoms. Now using equation (8) and the definition of T_1 we have

$$\ell s = T_1 V_F = T_2 V_F = \frac{1.1 V_F}{\gamma \Delta H} \qquad (11)$$

Taking equations (9) and (10) we get

$$\sigma = \frac{\gamma}{1.1 N_o V_F} \frac{\partial \Delta H}{\partial C} \qquad (12)$$

The experimental values for $\frac{\partial \Delta H}{\partial C}$ and the corresponding value of σ_{sf} are given in Table III. Figures 31 and 32 show these points along with data on other impurities obtained by ABS. The solid curve drawn in Figure 31 represents a two parameter fit made by Ferrel and Prange.[9] It should be noted that in their discussion FP stressed that a predicted spin-flip scattering cross section of $(4 \pm 1) \times 10^{-17}$ cm^2 for bismuth was a crucial test of their "resonance" hypothesis. The cross section of $(.73 \pm .3) \times 10^{-17}$ cm^2 obtained by means of high temperature techniques is somewhat lower than their value. However this comparatively low value for a high relative valence impurity does emphasize the resonant type behavior of Asik's results. A more detailed analysis of the resonance hypothesis will be given in the following section.

Figure 31. The valence dependence of the spin-flip scattering cross section of silver row impurities in sodium.

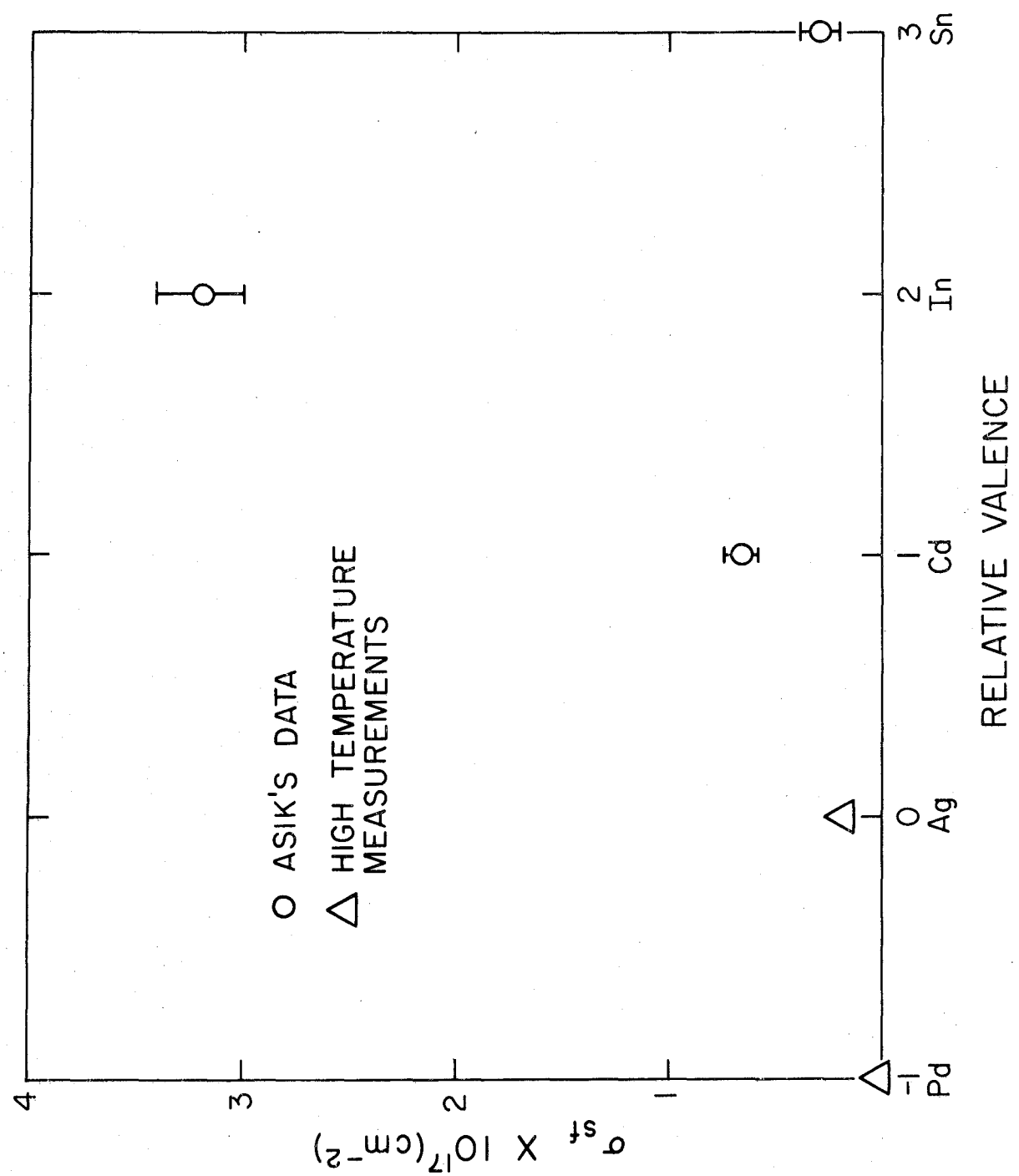
σ_{sf} X $10^{17}(cm^{-2})$
4
3
2
1
O ASIK'S DATA
△ HIGH TEMPERATURE MEASUREMENTS
-1 Pd
0 Ag
1 Cd
2 In
3 Sn
RELATIVE VALENCE

Figure 32. The valence dependence of the spin-flip scattering cross section of gold row impurities in sodium.

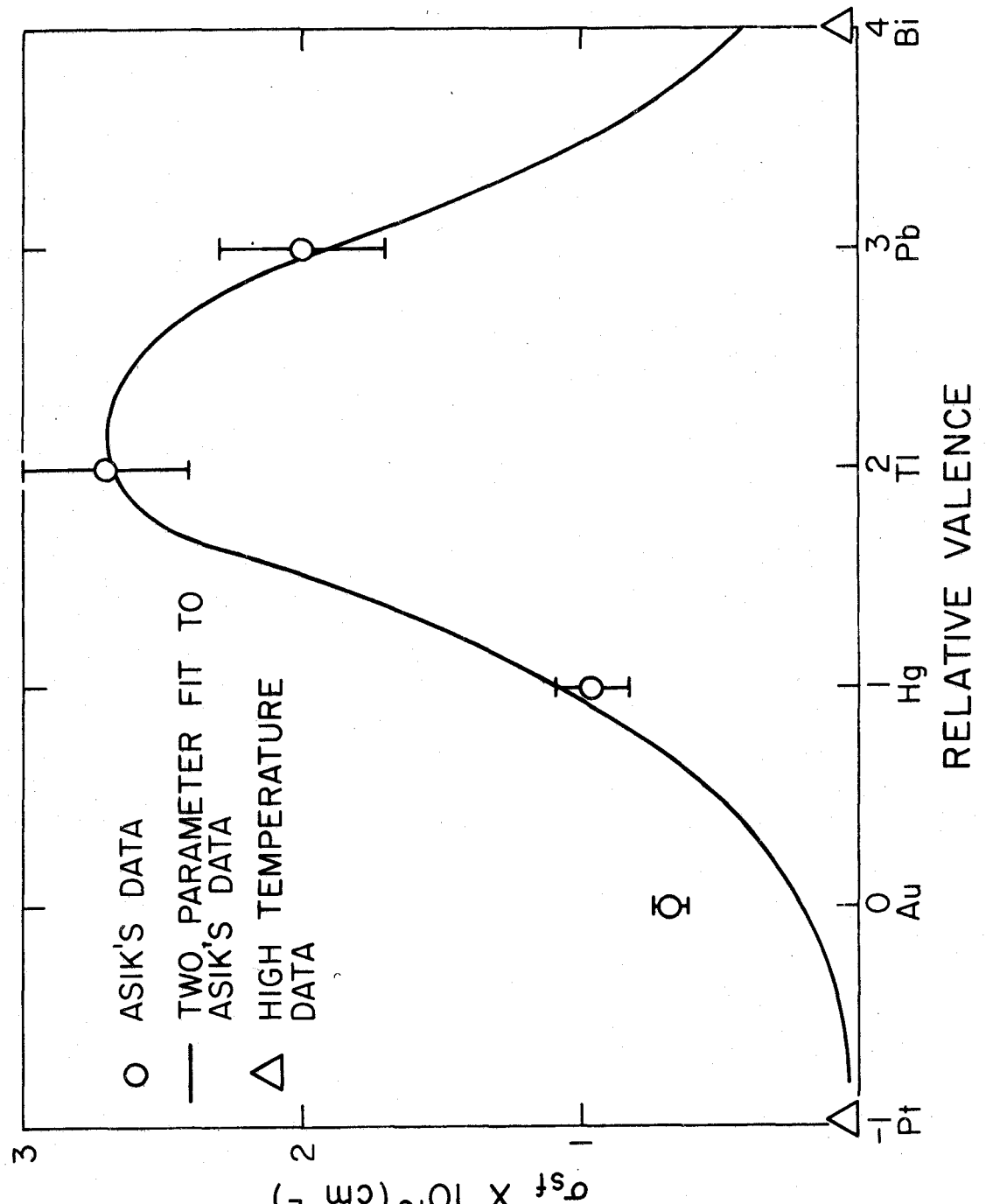
ASIK'S DATA
TWO PARAMETER FIT TO ASIK'S DATA
HIGH TEMPERATURE DATA
σ_{sf} X 10^{16} (cm^{-2})
RELATIVE VALENCE
Pt
Au
Hg
Tl
Pb
Bi

Table III.

Experimental Broadening Factor and Spin-Flip Scattering Cross Sections for Impurities in Sodium

Impurity	$\frac{\partial \Delta H}{\partial C}$	σ_{sf}
Bi	$(1.25 \pm .1) \times 10^{6}$	$(7.3 \pm .3) \times 10^{-18}$
Pt	$(5.8 \pm .3) \times 10^{5}$	$(3.4 \pm .2) \times 10^{-18}$
Pd	$(7.3 \pm .1) \times 10^{5}$	$(4.3 \pm .06) \times 10^{-19}$
Ag	$(3.0 \pm .2) \times 10^{5}$	$(1.8 \pm .1) \times 10^{-19}$

V. RESONANT SCATTERING

The process of putting an impurity atom into a metal is much like the problem of the contact potential between two metals. In the latter case a surface charge distribution develops to bring the two Fermi levels into register. For the impurity atom a "screening charge" develops which displaces the free atom energy levels relative to the metallic Fermi energy. As a rough rule of thumb, the free atom valence electrons levels are brought opposite the Fermi level. This corresponds to the situation in which the impurity is nearly electronically neutral. This condition of electrical neutrality can be succinctly expressed in terms of the change in partial wave phase shifts introduced by the potential around the impurity. This is a self-consistancy condition on the potential, and is known as the Friedel sum rule.

$$Z = \frac{2}{\pi} \sum_{\ell} (2\ell + 1)\, \delta^{\ell} \tag{13}$$

δ^{ℓ} is the partial wave phase shift for angular momentum ℓ, and Z is the valence of the impurity atom relative to the host metal.

The problem may be viewed by saying the valence states couple strongly to the conduction band states in the vicinity of the Fermi energy. As a simple model take the spherical square well potential in Figure 33 which has a bound state p level at E_p. Modifying this potential by making the wall a finite thickness as shown in Figure 34 allows the p state to couple with the free particle states outside the well whose energies are close to E_p. Incident electrons being scattered by this potential exhibit a resonance in their scattering cross section when

their energies coincide with E_p. Physically, one might say that an incident particle which has the right energy to couple into the potential tends to concentrate there. This produces large distortions in the wave function and hence a large amount of scattering.

The scattering cross section can be expressed in terms of the partial wave phase shifts.

$$\sigma = \frac{4\pi}{k_F^2} \sum_{\ell} (2\ell + 1) \sin^2\delta_\ell \qquad (14)$$

For p waves the cross section reaches a maximum when δ_1 is $\pi/2$. This occurs when the energy of the incident particle coincides with E_p. Below and above E_p, δ_ℓ is zero and π respectively. Figure 34 shows a typical phase shift curve. If the spin-orbit coupling between the electron and the impurity potential is included, the p level will be split into two as shown in Figure 35. These two new levels correspond to total angular momentum j being 3/2 and 1/2 and are split by roughly the spin-orbit coupling energy E_{so}.

In the case of impurity atoms in a metal only the electrons at the Fermi energy enter into the scattering. Thus information about only one point in the phase shift curve can be obtained. However, suppose that the depth of the square well is changed slightly from a value of V_1 to V_2. As shown in Figure 36 a new phase shift curve is generated which is displaced from the original one. Likewise the phase shift at the Fermi energy will be shifted. By varying the potential well depth a whole family of phase shift vs E_k curves can be generated. The intersections of these curves with the Fermi energy generate a phase shift vs well

depth curve. This situation can be expressed by writing the phase shift as a function of both E_k and V ($\delta^{\ell}(E_k,V)$). For an impurity atom in a metal, E_k is fixed at the Fermi level E_f by the host lattice. V is characteristic of the impurity and changes from one type to the next. If one assumes that only p screening is changing, then moving across the periodic table constitutes changing the impurity potential so as to produce a change in δ^1 of $\pi/6$ for each change in p valence electron. Assuming that the potentials of impurities from adjacent positions in the table are similar in shape but differ in depth V, one can think in terms of generating a phase shift vs V curve as is shown in Figure 36. It is the shape of this curve that determines how spin flip scattering behaves as a row of the periodic table is traversed. Assuming that the spin-orbit coupling is small one can write

$$\delta^{\ell}_{\ell-1/2} - \delta^{\ell}_{\ell+1/2} = E_{so} \frac{\partial \delta^{\ell}(E_k,V)}{\partial V} \tag{15}$$

Considering only p terms, equation (1) for the spin-flip scattering cross section becomes

$$\sigma_{sf} = \frac{16}{9} \frac{\pi}{k_F^2} \sin^2 \left(E_{so} \frac{\partial \delta(E_F,V)}{\partial V} \right) \tag{16}$$

Comparing equations (14) and (16) it is noted that spin flip scattering differs from momentum scattering in that it depends on the derivitive of δ^{ℓ} rather than on δ^{ℓ}. Consequently a maximum in σ_{sf} occurs at a point of maximum slope where a maximum in resistive scattering occurs at $\delta^{\ell} = \pi/2$. According to the Friedel sum rule this corresponds to a relative p valence of +3.

Figure 33. Spherical square well potential.

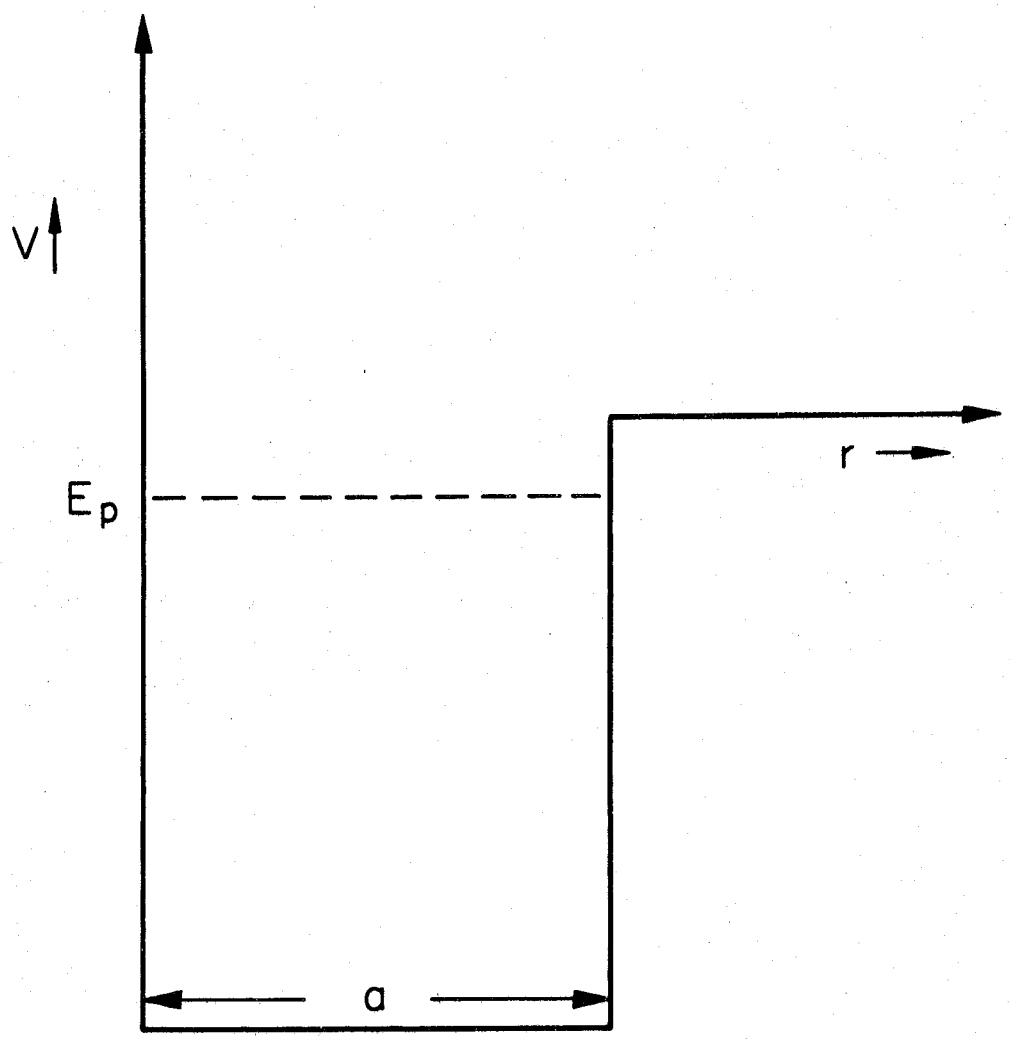
V
r
E_p
a

Figure 34. Spherical potential well with finite wall showing p wave phase shift.

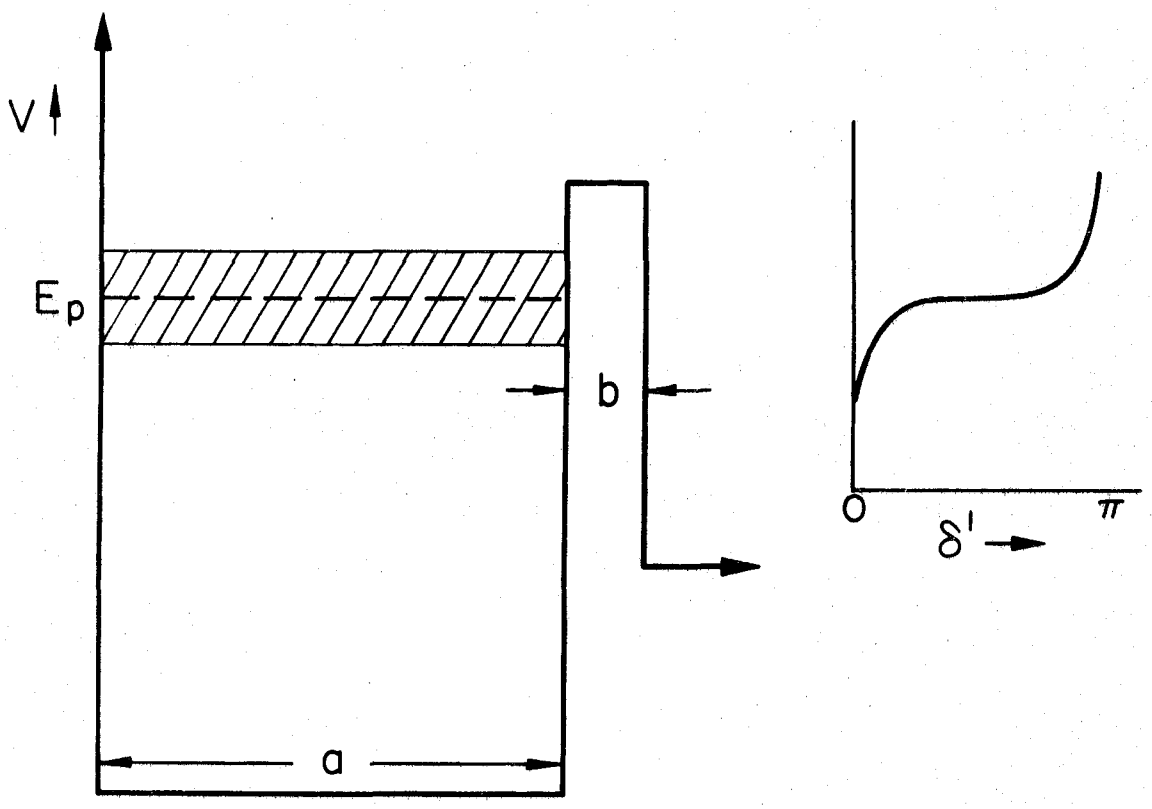
V
E_p
b
a
0
π
δ'

Figure 35. Potential well with finite wall and spin-orbit splitting of p state.

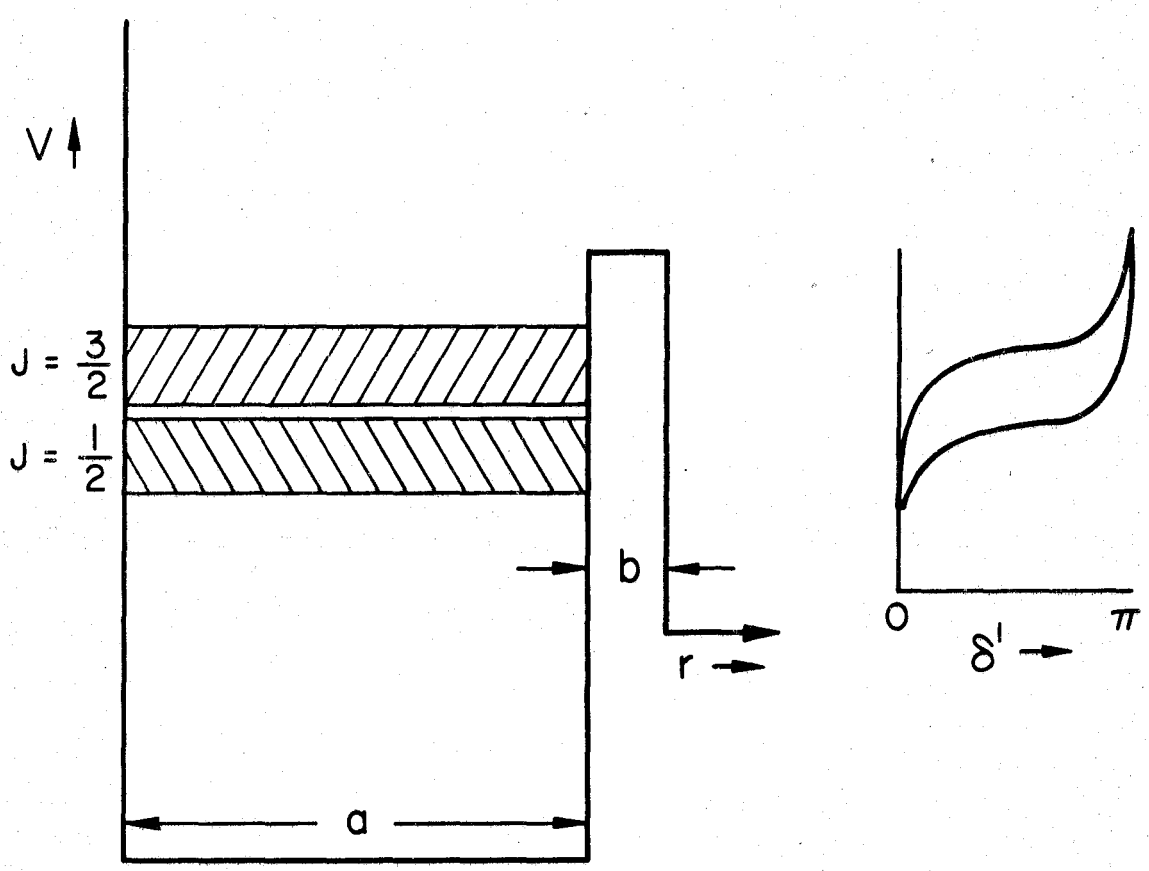
V
J = 3/2
J = 1/2
b
r
a
0
π
δ'

Figure 36. Phase shift curves as a function of E_k and V.

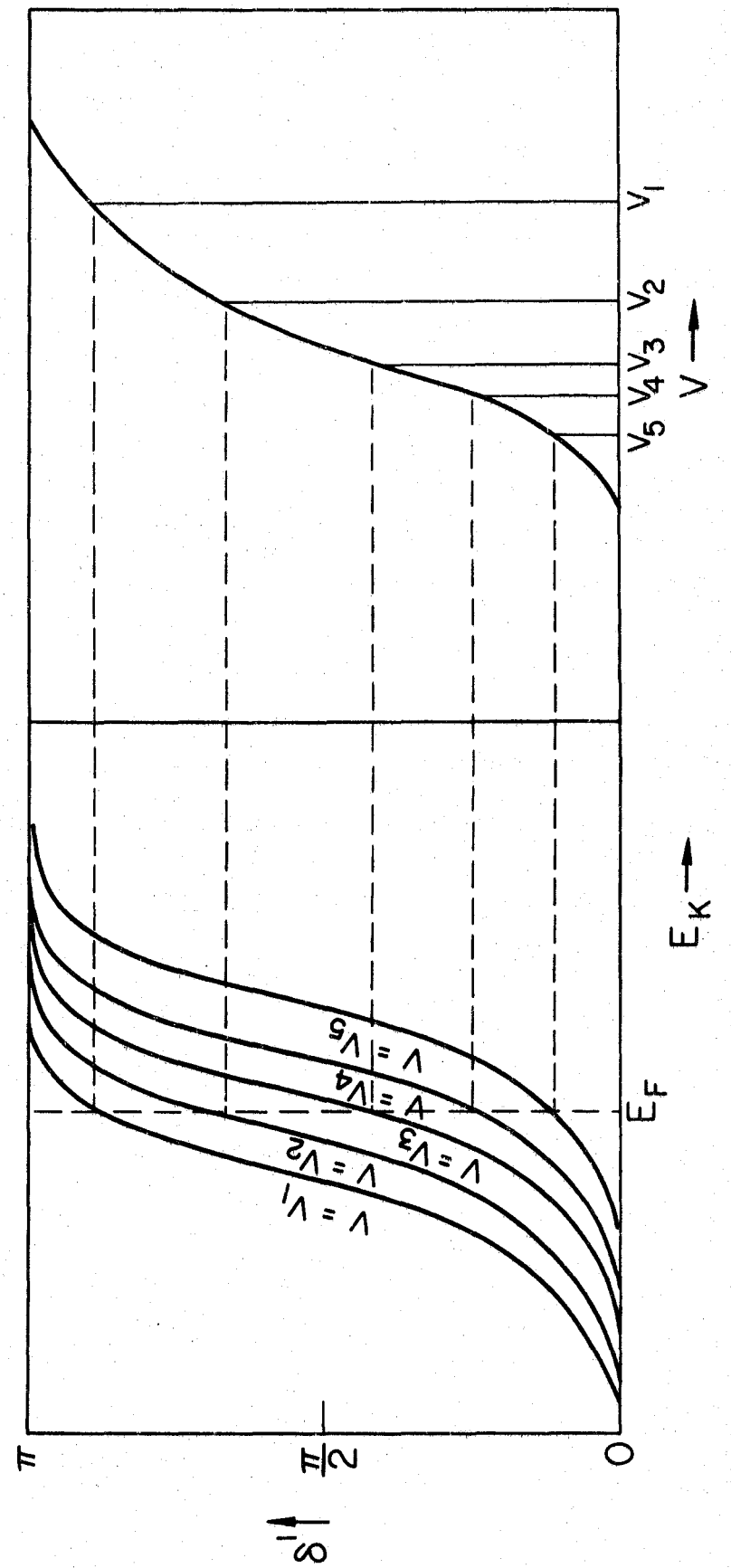
V_1
V_2
V_3
V_4
V_5
V
E_K
E_F
$V = V_5$
$V = V_4$
$V = V_3$
$V = V_2$
$V = V_1$
π
π/2
0
θ

Ferrel and Prange[9] have analysed spin flip scattering data on silver and gold row impurities under the hypothesis that the p wave phase shift manifests a sharp resonance as the row is traversed. As is customary for sharp resonances, FP characterize the phase shift dependence on E_k as

$$\delta^1 = \tan^{-1}\left(\frac{\tau}{2(E_k - E_p)}\right) \tag{17}$$

where τ is the resonance width and E_p is the level of the resonance energy. To obtain the V dependence of δ^1 they assume that the same shape is transferred to the δ^1 vs V curve. In the case of the square well model, this is a valid approximation if the resonant energy level, E_r, remains a fixed distance from the bottom of the well. Introducing an arbitrary shift Z_o in the Friedel sum rule corresponding to screening by other angular momenta, equation (16) becomes

$$\sigma_{sf} = \frac{16\pi}{k_F^2}\left[\left(\frac{2E_{so}}{\tau}\right)^2 \sin^2\left(\frac{\pi}{6}(Z - Z_o)\right)\right] \tag{18}$$

The results of a two parameter least squares fit of this equation to ABS's experimental data is shown in Figure 32. FP were not able to fit the data in Figure 31. The central point, the cross section for indium, is too high to be consistent with the neighboring points of cadmium and tin to be fitted by equation (18).

The main difficulty with FP's approach is its requirement of a p wave phase shift of $\pi/2$ for s^2 and s^2p electronic configurations. Odle and Flynn,[27] in work on Knight shift in liquid alloys of copper with

copper row impurities, found it consistent with their data to assume the quantity of screening for an impurity atom dissolved in a metal to be approximately the same as that in the free impurity atom.

$$Z_\ell = \frac{2}{\pi} (2\ell + 1)\ \delta^\ell \tag{19}$$

Resistivity measurements concur with this observation.[21,22]

FP have used equation (17) as an approximation for the phase shift under the resonance hypothesis. This equation is only accurate in so far as the width τ is small compared to the Fermi energy. The values of τ that FP obtained from their curve fitting are 3.2 eV and 4.2 eV for thalium and indium in sodium. When compared to a sodium Fermi level of 3.1 eV this seems to indicate that the sharp resonance assumption is not valid. In order to understand how a large value of τ/E_f would effect the shape of the phase shift curve consider a modified spherical square well potential shown in Figure 37. The "lip" was added in order to have a means of adjusting the width of the resonance. Figure 38 shows the p wave phase shift resulting from this potential in the case where $\tau/E_f \approx 1$. The maximum slope occurs at $\delta^1 = \pi/2$. This corresponds to a maximum spin-flip scattering cross section at a relative valence of 1.5. It should be noted however, that since this phase shift curve reaches a maximum of $.65\pi$ (which corresponds to 3.2 p electrons) it cannot represent the filling of a p-shell which requires a phase shift of π for the six electrons. This curve does indicate however, that a more complex form of equation (17) must be used.

The resonance hypothesis is capable of explaining the existence and to some extent the shape of the scattering peak. However the

Figure 37. Modified square well potential.

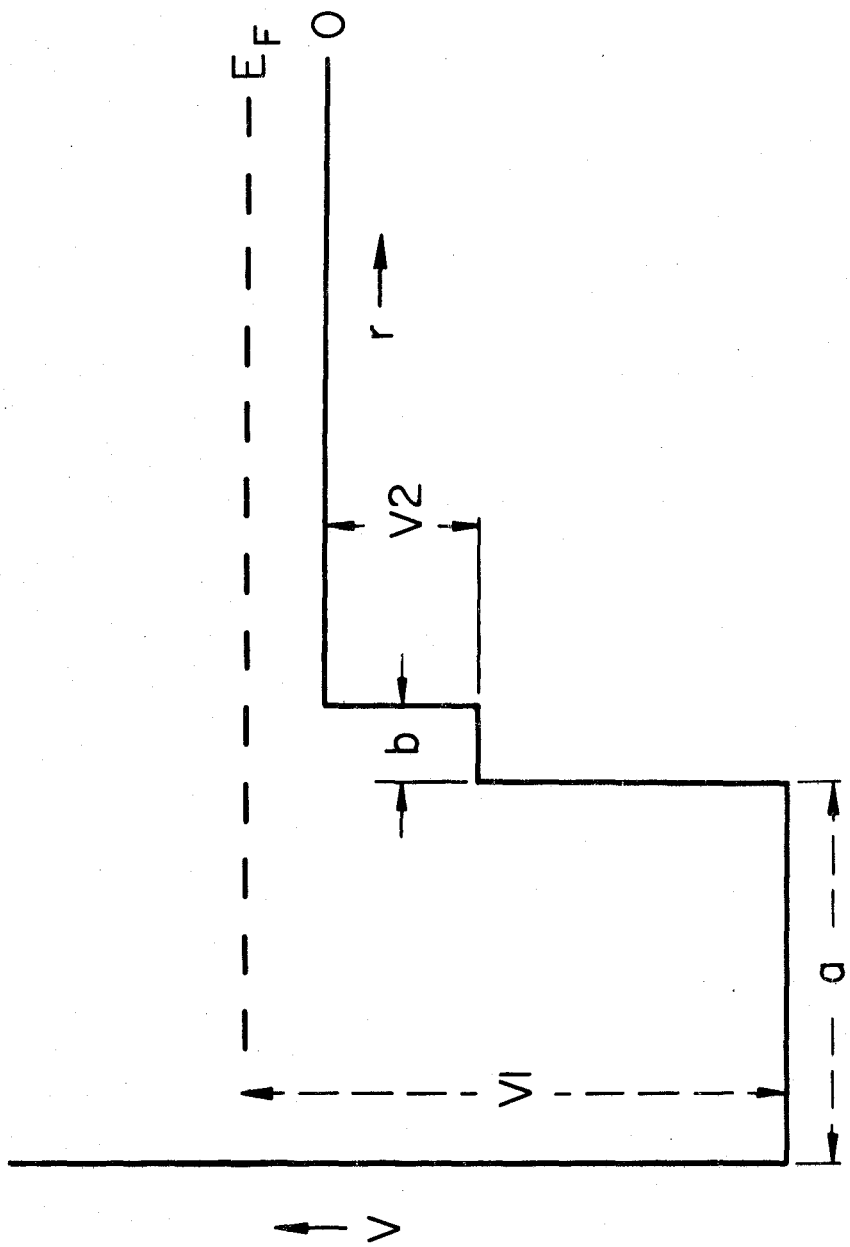
E_F
O
r
V2
b
a
V1
V

Figure 38. P wave phase shift for modified square well potential.

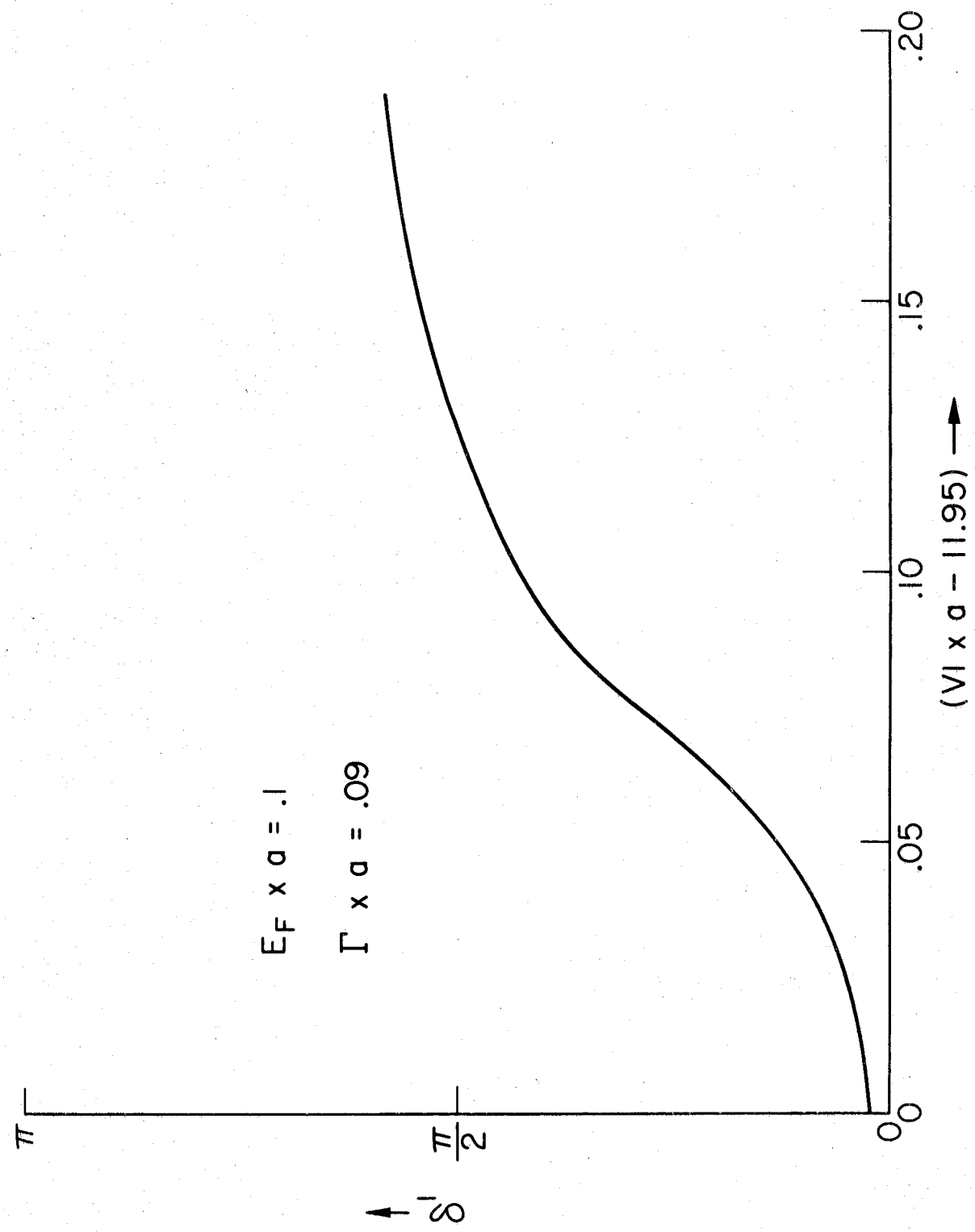
$E_F \times a = .1$
$\Gamma \times a = .09$
δ_-
π
$\frac{\pi}{2}$
0
0
.05
.10
.15
.20
(VI x a − 11.95) ⟶

question of position is still unanswered. If one is to accept that an electronic configuration of s^2p^3 corresponds to a p phase shift of $\pi/2$. then a more detailed description of the structure of the resonance is needed. If on the other hand, the FP description is accepted then the burden of understanding is shifted to determining why a p-wave phase shift of $\pi/2$ occurs for electronic configurations of s^2 and s^2p. One possible mechanism for this is a repopulation effect in which the p-wave phase shift is increased at the expense of the s and d phase shifts. If the s and d states move up to the Fermi surface their phase shifts will decrease and the Friedel sum rule requires the p-wave phase shift to increase. A charging effect described theoretically by Stern[40] may also give rise to a repopulation. He shows that the constituents of alloys in general have a different number of tight binding approximation electrons than the pure metals. Since the resulting electronic distribution due to the charging effect must conform to the Friedel sum rule, any charge transfer will involve changing the s, p, and d partial waves.

It is possible that both of these approaches discussed above are correct and can account for the behavior of the σ_{sf}. Further experimental information on impurity induced resistivity and Knight shift changes would help in determining the true mechanism.

REFERENCES

1. Metallic Solid Solutions, edited by J. Friedel and A. Guinier (W. A. Benjamin, New York, 1963).
2. J. F. Blatt in Solid State Physics, edited by F. Seitz and D. Turnbull (Academic Press, New York, 1957), vol. 4.
3. C. Kittel, Quantum Theory of Solids (John Wiley and Sons, New York, 1963), chap. 18.
4. C. Kittel, Quantum Theory of Solids (John Wiley and Sons, New York, 1963), chap. 18.
5. N. S. Garifianov and M. A. Storikov, Zh. Esperim. i. Teor. Fiz. 35, 798 (1958) [English transl.: Soviet Phys. - JETP 8, 553 (1959)].
6. G. D. Wignall, J. E. Enderby, C. E. Hahn and J. M. Titman, Phil. Mag. 12, 433 (1965).
7. J. Friedel, Phil. Mag. 43, 153 (1952).
8. J. R. Asik, M. A. Ball, and C. P. Slichter, Phys. Rev. Letters 16, 740 (1966). The initials ABS shall refer to this work.
9. R. A. Ferrel and R. E. Prange, Phys. Rev. Letters 17, 699 (1966). The initials FP shall refer to this work.
10. J. R. Asik, Thesis, University of Illinois, (1966).
11. T. W. Griswold, A. F. Kip, and C. Kittel, Phys. Rev. Letters 88, 951 (1952).
12. C. Feher and A. F. Kip, Phys. Rev. 98, 337 (1955).
13. R. A. Levy, Phys. Rev. 102, 31 (1956).
14. S. Schultz and M. R. Shanabarger, Phys. Rev. Letters 16, 178 (1966).
15. W. M. Walsh, Jr., L. W. Rupp, Jr., and P. H. Schmidt, Phys. Rev. Letters 16, 181 (1966).

16. S. Schultz and C. Latham, Phys. Rev. Letters 15, 148 (1965).

17. S. Schultz, G. Dunifer, and C. Latham, Physics Letters 23, 192 (1966).

18. S. Schultz and M. R. Shanabarger, Phys. Rev. Letters 19, 749 (1967).

19. J. Asik, M. Ball and C. P. Slichter, Phys. Rev. Letters 16, 740 (1966).

20. R. A. de Casteljan De faget and F. Friedel, Jour. Phys. Rad. 17, 27 (1956).

21. C. R. Vassel J. Phys., Chem. Solids 7, 90 (1958).

22. C. B. Coqblin, J. Delaplace, V. Levy, A. A. Gomes, and J. Hillairet, Journal de Physique 28, 75 (1966).

23. K. C. MacDonald, W. B. Pearson and I. M. Templeton, Phil. Mag. 6, 1431 (1961).

24. D. W. Bridgmen, Proc. Am. Acad. 83, 149 (1954).

25. J. F. Freedman and W. D. Robertson, J. Chem. Phys. 34, 769 (1961).

26. K. Borneman and W. D. Rauschenplat, Metallurgie 9, 473 (1912).

27. R. L. Odle and C. Flynn, Phil. Mag. 13, 699 (1966)

28. M. Hanabusa and N. Bloembergen, J. Phys. Chem. Solids 27, 363 (1966).

29. The basic design for this cavity was first proposed by L. S. Singer. [L. S. Singer, Review of Scientific Instruments 32, 213 (1961).

30. Platinum paste No. 6082 manufactured by the Hanovia Liquid Gold Division of Englehard Industries, Inc.

31. J. R. Asik, Thesis, University of Illinois, (1966).

32. Liquid Metals Handbook edited by C. B. Jackson (U.S. Government Printing Office, Washington, D.C. 1955).

33. M. H. Cohen and V. Heine, Advances in Physics 7, 395 (1956).

34. A. S. Nowick and J. F. Freedman, Acta. Met 6, 176 (1958).

35. W. Seith and O. Kubaschewske, Z. Electrochem 43, 743 (1937).

36. W. Hume-Rothery, Electrons, Atoms, Metals and Alloys (Dover Publications, New York 1963, 3rd ed.).

37. F. J. Dyson, Phys. Rev. 98, 345 (1955).

38. R. T. Carver and C. P. Slichter, Phys. Rev. 102, 975, (1956).

39. Y. Yafet in Solid State Physics, edited by F. Seitz and D. Turnbull (Academic Press, New York, 1963), vol. 14.

40. E. A. Stern, Physics 1, 255 (1957).

VITA

Edward Kevin Cornell was born on December 10, 1941 in New York, New York. He graduated from the Putney School, Putney, Vermont in June, 1959 and in June, 1963 received his Bachelor of Arts degree from Swarthmore College, Swarthmore, Pennsylvania. In June, 1963 he married Nina Wilson. He entered the Graduate College of the University of Illinois in September, 1963 and received the Master of Science degree in February, 1965. During the academic year 1965-66 he held a General Electric Company Fellowship. From 1966 to 1967 he held a Minnesota Mining and Manufacturing Fellowship. For the remainder of the time Mr. Cornell has received financial support in the form of teaching and research assistantships. He is a member of the American Physical Society.